University of Notre Dame
Notre Dame, Indiana 46556

SEMI-ANNUAL STATUS REPORT
for the
Period Ending May 30, 1989
for
NASA GRANT NSG 1419*

All of the time and effort during this report period was directed toward obtaining and analyzing LDV data, obtaining static pressure data, and using smoke flow visualization to correlate separation bubble data. The study focused on the Eppler 387 airfoil at a chord Reynolds number of 100,000 and an angle of attack of 2°. Additional data was also obtained from the NACA 663-018 airfoil at a chord Reynolds number of 160,000 and an angle of attack of 12°.

This research has as its objective the detailed documentation of the structure and behavior of the transitional separation bubble and the redeveloping boundary layer after reattachment over an airfoil at low Reynolds numbers. The intent of this work is to further the understanding of the complex flow phenomena so that analytic methods for predicting their formation and development can be improved. These analytic techniques have applications in the design and performance prediction of airfoils operating in the low Reynolds number flight regime.

INTRODUCTION

The interdependence of the flow field characteristics of low Reynolds number aerodynamics such as laminar separation, transition, turbulent reattachment, and turbulent separation has slowed the formulation of empirical and analytical models. Accurate experimental results are useful for development of new models and comparison with computational results.

Increasing the low Reynolds number data base was the primary function of the research supported by this grant. Boundary layer data for this purpose was obtained by LDV measurements. The advantage of this method over the more commonly used hot-wire anemometry method is the ability to discern flow direction and magnitude unobtrusively and directly. Data for two airfoils supporting two different types of laminar separation bubbles was obtained. Measurements on the Eppler 387 airfoil include LDV boundary layer profiles at R_c = 100,000 and α = 2.0° across the upper surface, with particular emphasis on the bubble region. The conditions and model size, chord = 304.8 mm, were chosen to give a large steady bubble. LDV boundary layer measurements were also made on the upper surface of a NACA 663-018 airfoil at R_c = 160,000 and α = 12.0°. This exact airfoil model has previously been used at Notre Dame with hot-wire and LDV techniques.

---

* NASA Technical Monitor for this Grant is Mr. Robert J. McGhee, NASA Langley Research Center, Hampton, VA 23665

The results of this research are presented with particular emphasis on measurement uncertainty and errors. The low Reynolds number regime provided a challenge for the measurement techniques used. Some of the factors involved include low velocities, small physical dimensions, and unsteadiness in the flow field of interest.

Airfoil Models

The Eppler 387 airfoil models were constructed in the Aerospace Laboratory shop by machining an aluminum master plug and constructing molds from which models could be cast in epoxy. The airfoil models used had a 0.3048m chord and quarter chord sting mount location and various spans. The coordinates for the Eppler 387 airfoil were provided by NASA Langley. Three models were used in the various tests. The surface/smoke flow visualization and pressure models had a 0.406m span. These models were mounted centered in the tunnel cross section between 0.61m x 0.61m plexiglass endplates. These endplates featured round leading and square trailing edges and located the airfoil quarter chord location 0.267m from the leading edge of the endplate. The pressure model included 66 ports for static pressure measurement. These ports were 0.79mm in diameter and were normal to the airfoil surface. All ports led into Teflon tubing of 1.78mm O.D. and 1.27mm I.D.. Port positions were staggered along the span at a 60° angle to the leading edge. This was done to reduce port disturbance effects of upstream taps. The LDV model extended from one tunnel side wall to the other with a 0.61m span.

EXPERIMENTAL RESULTS

The goal of this research was to document the laminar separation bubble on the Eppler 387 airfoil. Measurement difficulties and uncertainty at low Reynolds numbers were given special attention. The data includes static pressure and LDV measurements as well as flow visualization photographs. Experimental data is useful for computational code verification and bubble model development. These codes (examples: Drela, 1987, 1989, and Eppler, 1986) often utilize empirical and semi-empirical models of the laminar separation bubble transition process. In addition, experimental data, especially data taken at several facilities, allows for a better understanding of the effects of tunnel environment on low Reynolds number airfoil performance.

Static Pressure Data

The static pressure measurements were made to locate the position of the bubble. This was done to verify certain aspects of the research. The locations of laminar separation, transition, and turbulent reattachment are sensitive to tunnel turbulence intensity as well as airfoil model accuracy and surface finish. Comparison of these results was made with the results obtained by McGhee (1988) in the LTPT at NASA Langley.

The data is presented uncorrected and as such is distorted slightly due to the finite size and constrained nature of the wind tunnel flow field. This data is intended to help document the flow

field which contains a laminar separation bubble. Presented as such it is ideal for comparison with previous data, often presented uncorrected, taken at the Notre Dame wind tunnels. In particular it should be compared with data taken on similarly sized models some of which have supporting LDV data. Data at large angles of attack (>10.0°) was not taken because of the large model size and ensuing flow field distortion.

Static Pressure Measurement Error Analysis

The static pressure measurement uncertainty varied with the magnitude of the pressure and thus varied with angle of attack and Reynolds number. The largest uncertainties were present for high α and low Reynolds number. A representative value for the largest uncertainty was ΔC_p =0.1796 for R_c=75,000 and α=8.0°. In contrast uncertainty could be as low as ΔC_p =0.0072 for R_c=300,000 and α=0.0°. Uncertainty in C_p varied along the chord with variations in C_p. ΔC_p was largest for low freestream velocity and high airfoil static pressure. Pressure distribution repeatability is shown in Figure 1 for four different tests at R_c=100,000 and α=2.0°. Two of these tests were specifically made to determine if hysteresis was present. The four plots for the tests group closely, almost within the uncertainty, which is ΔC_p=0.0496 for this case. The discrepancies are probably the result of uncertainty in angle of attack ($\Delta\alpha$ = 0.15°) and variations in Reynolds number (approximately ±2%) during the testing.

Figure 2 shows a comparison of pressure distributions measured at Notre Dame and NASA Langley at R_c=100,000 and α=2.0°. Notice the data sets exhibit the same stagnation points. Also the locations of separation, transition, and reattachment are nearly coincident. These sets of data exhibit an offset or a difference in C_p of about 0.057. If these pressure distributions are integrated for lift coefficient this offset is irrelevant. Integration of these data sets by the same program results in identical lift coefficients of C_L=0.611 . The cause of the offset is unknown. Previous tests (Brendel 1986) have shown the time constant for the tubing used in the pressure measurements to be on the order of 60 msec. A delay of over 16 time constants was used before measurements were recorded so pressure attenuation in the tubing should be small. It also seems unlikely that the offset is a result of a manometer calibration problem as manometer calibration was checked. A discrepancy in angle of attack may explain this offset. A maximum angle error between the airfoils tested in the two wind tunnels would be the sum of the angle of attack uncertainties. An estimated value for this uncertainty is twice the uncertainty for the Notre Dame data. This value would then be $\Delta\alpha$ = 0.30°.

Lift curve slopes for identical airfoils tested in different facilities often contain discrepancies. It is possible that the flow environment or model differences could cause such an effect by altering the laminar separation bubble. A higher value of free stream turbulence intensity often acts like an increase in Reynolds number. This would shorten the bubble, altering the pressure distribution. The pressure distribution would likely show a more negative pressure peak.

Another explanation may be tunnel wall interference but the expected trend for this would be pressure distribution distortion. A similar situation existed in comparing data from the Notre Dame wind tunnel to data taken in free flight. These pressure distributions from the free flight test showed lower values of C_p across the chord on the upper and lower surface. Lower values of C_p across the chord was the same trend seen between the NASA Langley data and the Notre Dame data. In the pressure distributions, lower values of C_p are higher on the graph as negative C_p is plotted on the positive y axis.

A summation of separation, transition, reattachment, and attached transition is shown in Figures 3 to 5 for Reynolds numbers of 100,000, 200,000, and 300,000 respectively. These locations were determined from the pressure distributions and have an uncertainty of ±1% x/c. The locations of attached transition were taken from Eppler's program results (Eppler, 1986). The data for R_c=100,000 is shown in Figure 3 . This figure shows the long bubbles that form on the E387 airfoil at moderate angles of attack. As angle of attack increases the bubble moves forward and shortens in length. At an angle of attack of seven to eight degrees the bubble location moves rapidly forward to near the leading edge were a short bubble is formed. This is the same angle for which an attached transition process is seen at higher Reynolds numbers. The population of data points for the higher Reynolds numbers is sparse but the trend of bubble shortening and migration forward can still be seen. The attached transition process is represented by a single symbol for transition. At the higher Reynolds numbers the location of the short leading edge bubble is not shown due to the poor position resolution caused by tap spacing.

Lift and Moment Curves

The measured pressure distributions were integrated for lift and quarter chord moment. The resulting coefficients do not have standard tunnel corrections applied. The worst case uncertainty in lift and moment coefficient was approximately twice the average uncertainty in pressure coefficient for a particular test case. This results in a representative uncertainty in lift coefficient, ΔC_L, of 0.1 for R_c=100,000 and α=2.0°. The uncertainty in lift coefficient dropped to approximately ΔC_L=0.02 for R_c=200,000. The uncertainty in moment coefficient may be assumed to on the same order as that for the lift coefficient. Uncertainty in pressure tap location was not known. This value could be assumed to be on the order of the tap hole diameter, which was .79 mm, for the chord wise coordinate, but was unknown for the other coordinate. Figure 6 shows the lift and moment curve slopes for the E387 airfoil at a Reynolds number of 100,000. The two sets of data come from Notre Dame and NASA Langley. The lift curves match well. The start of nonlinearity in the lift curve slope at high angle of attack is pronounced and both data sets agree in this respect. The linear portion of the curves seem to differ in slope with the lift curve slope of the Notre Dame data being the greater of the two. Lack of tunnel corrections could possibly account

for this. The moment curves compare poorly but the same trend toward reduced negative pitching moment at high angles of attack is shown by both data sets.

Laser Doppler Velocimetry Boundary Layer Measurements

Boundary layer measurements by LDV are attractive in flow fields with reverse flow like that inside laminar separation bubbles. These measurements were made on the E387 airfoil at R_c=100,000 and α=2.0°. The LDV data for R_c=100,000 and α=2.0° is plotted in dimensionless U/U_{ext} velocity plots. In these plots the vertical distance, y (mm), is normal to the airfoil's surface. The chord position is set manually and uncertainty in chord position is estimated to be about 1 mm or 0.33% x/c. This uncertainty arises from a combination of possible errors that include scribed airfoil chord locations and initial probe volume location.

Figures 7-9 show laminar boundary layers upstream of the laminar separation bubble. The pressure gradient on the E387 at these conditions is favorable up to 25% x/c and adverse after this chord station. The boundary layers in Figure 9 are for 38% x/c and 39% x/c and show the effects of an adverse pressure gradient with thicker boundary layers. The 39% x/c profile in Figure 9 b) shows near separation like behavior with an inflection point and small velocity gradient dU/dy at the surface. Figure 10 a) shows the velocity profile at 40% x/c to be the first separated velocity profile. This profile also exhibits reverse flow. The separation point is now determined by LDV data to occur at 39.5% ± 0.8% x/c.

A distinct region of the bubble is located from separation to 55% x/c. In this laminar region a distinct recirculation zone is seen. Figures 10-13 show these profiles. If the pressure distribution in Figure 14 for R_c=100,000 and α=2.0° is examined the region from separation to 55% x/c shows a slight pressure recovery with a small adverse pressure gradient. The LDV measurements in this region were made with relatively good seeding and are presented with relatively good confidence (i.e., accurate to with ±15%).

The velocity profiles downstream of this recirculation region show very little reverse flow as can be seen in Figures 15-17 for chord stations of 56% to 66% x/c. As previously mentioned the seeding for LDV measurements in this region was poor. The pressure distribution over this region shows a pressure gradient that is very nearly zero. This plateau of zero pressure gradient roughly extends from 54% x/c to 76% x/c. Flow visualization photographs show a possible Tollmein-Schlichting disturbance that is first noticed around 66% x/c.

The pressure distribution in Figure 14 suggests transition to turbulent flow in the shear layer at 76% x/c. This is the beginning of the rapid pressure recovery region of a turbulent boundary layer. The velocity profiles from 68% x/c to 74% x/c show odd shapes as seen in Figures 18 and 19 . This may be a result of improper bandpass filtering in the LDV measuring process or a velocity bias. A velocity due to fluctuating flow would be towards higher velocities. Considering the possibility of improper filtering and poor seeding these profiles may yet show a

possible boundary layer profile. The flow in this region may contain circulation. The net flow through this aft region of the bubble may be nearly zero, yet instantaneous streamwise and reverse flow with a recirculation pattern may be present periodically. The boundary layer measurements are a long term average of this behavior so actual average measurements of reverse flow may be unlikely. Vorticity seems to be shed from the shear layer during transition, a point located above the airfoil surface. This corresponds with the shape of the profiles which suggest a core location about 3.5 mm above the surface at 70% x/c and about 6 mm at 74% x/c. This vorticity is rapidly dissipated and is not seen at 76% x/c.

The shear layer grows rapidly after transition and the boundary layer profile at 76% x/c shown in Figure 20 a) shows this. The profile exhibits reverse flow but the boundary layer thickness is very low, just over 2mm. This can be compared to the boundary layer thickness at 68% x/c which is over 6.5mm. The profiles at 78% x/c and 80% x/c shown in Figure 20 b) and 21 a) show nearly attached boundary layers. The profile at 81% x/c in Figure 21 b) is the first measured attached boundary layer after the bubble. LDV measurements suggest the reattachment location to be 80.5% ±.8% x/c. Figure 22 shows turbulent boundary layers at 90% x/c and 95% x/c.

LDV Measurement Uncertainty and Repeatability

Uncertainty in LDV measurements by direct calculation for the system used would be complex. Such things as uncertainty in focal length and aberration for optics and uncertainty in laser light frequency or coherency would be hard to quantify. Other factors like uncertainty in shifting frequency and calibration of frequency shifting were not investigated. The LDV system should be accurate and repeatable, if properly adjusted, for measurements with good seeding in steady flows. Meyers (1979) listed LDV hardware uncertainty to be on the order of two and one half percent.

The quality of LDV measurements can be degraded by several measurement situations. Those pertinent to this experiment will be described. Low data density and its associated discontinuous signal, often found with poor or intermittent seeding, can result in velocity measurement errors. Fringe bias results when particles pass through the measuring volume fringes in a non-normal direction. This would be the case for boundary layer measurements in a laminar separation bubble. A bubble often contains recirculation regions and measurements with at fringe velocity vector angle up to 90° would seem probable. The probability of making a measurement decreases 10% when the velocity vector and the fringe normal differ in angle by 37°. Fringe bias is reduced by frequency shifting and high cycles per burst criterion, both of which were used in the measurements presented in this thesis. Another bias is a velocity bias associated with fluctuating flows. In an unsteady flow a high flow velocity measurement is more probable than a low one as high velocities carry a greater number of particles through the probe volume. This results in an

erroneous average velocity measurement. In a LDV experiment conducted by Bogard (1979) on the viscous sublayer of a fully developed turbulent boundary layer in a channel, velocity bias errors of 10% were found. This was the difference between weighted and unweighted average velocity measurements. In Bogard's experiment LDV measurements were made with natural seeding in a water tunnel. Turbulence in the boundary layer was solely responsible for the bias. Velocity bias also can be attributed to multiple measurements on a single particle. Even the finite size of the probe volume contributes to velocity errors in a flow region with a velocity gradient. Meyers (1979) listed maximum errors in measured turbulence intensity up to 0.5% due to probe volume size alone.

Previous investigators (Fitzgerald, 1988 and Brendel, 1987) have compared low Reynolds number LDV boundary layer measurements to hot-wire measurements. Comparison is very good for nondimensional tangential velocity in the outer regions of the boundary layer and above. Fitzgerald listed the accuracy of velocity measurements as ±0.15 m/sec for the hot-wire and <10% for the LDV measurements. Fitzgerald also noted that U_e varied greatly from chord station to chord station. These uncertainty values seem overly optimistic.

The largest factor in LDV velocity measurement for this experiment was proper resolution of an average velocity in an unsteady flow with poor seeding. The type of flow inside a laminar separation bubble. Proper weighting factors for individual velocity measurements are needed to eliminate velocity biases. The proper bandpass filtering is easy to determine in attached laminar and turbulent boundary layers by observation of the doppler bursts in the photomultiplier signal. The proper filtering is more difficult inside the bubble due to nonuniform seeding of the flow with smoke particles. The initial laminar region of the bubble described earlier was unexpectedly easy to measure. The following region was more difficult, with very sparse seeding, but what seemed to be the best filtering was used. In this region average velocities near zero were often composed of individual velocities that ranged from -2 m/sec to 2 m/sec. The profiles in the turbulent aft region of the bubble usually provide good quasi-steady seeding. These profiles were measured and looked quite strange with a pronounced "s" shape. These profiles were remeasured with different bandpass settings and seemed to show a region that was forced to low velocity by the filtering process. The original measurements were thus retained.

Another source of error includes wind tunnel free stream variations. Considering all factors a value for uncertainty in LDV measurements is estimated to be $\Delta U/U_{ext} = .15$ inside the laminar separation bubble's boundary layer and ±15% above and outside the bubble. Because the average velocity inside the bubble, measurements below the displacement thickness, can vary from approximately -20% to 80% of U_{ext}, the estimated uncertainty can range from 20% to 75%. Confidence in measurements is increased if they are repeatable in the long term. Figure 23 shows two such repeatability tests. These profiles show worst case repeatability for profiles were filtering

and seeding was considered good. Both of these profile comparisons contain local areas were velocity measurements differed considerably. In general velocity profile measurements were repeatable to a difference less than 5%.

CONCLUSIONS

The objective of this study was to measure the flow field in and around the laminar separation bubble on an E387 airfoil at low Reynolds numbers. The measurements were made using LDV at R_c = 100,000 and α = 2.0°. Supporting static pressure measurements and flow visualization were also made. Static pressure measurements for the E387 airfoil at angles of attack from negative two to ten degrees at Reynolds numbers from 75,000 to 300,000 were made to locate the laminar separation bubble and were integrated for lift and moment curves.

The Eppler 387 exhibits a large laminar separation bubble at a mid-chord location for low angles of attack. At R_c = 100,000 and α = 2.0° this bubble extends from 39.5% ± .8% x/c to 81.5% ± .8% x/c as determined by LDV measurements. At these conditions the location of transition in the shear layer is at 76% ± .8% x/c as determined by the peak in displacement thickness calculated from LDV measurements.

A compilation of data obtained by the LDV method at low Reynolds numbers on airfoils with laminar separation bubbles is tabulated in Table I . Examination of this data reveals a few trends. The transition Reynolds number of the separated shear layer increases with increasing Reynolds number based on momentum thickness at separation. Brendel reached a similar conclusion and the new cases shown in Table I support this. This suggests that the transition Reynolds number parameter is not a constant as some investigators have suggested. The Reynolds number based on momentum thickness at separation provides a measure of the stabilizing effects that the airfoil's surface has on the separated shear layer.

Previous investigators (Fitzgerald 1988) found discrepancies in trends for integrated parameters between hot-wire and LDV data for the NACA 66_3-018 airfoil at R_c=140,000 and α=12.0°. New measurements on the NACA 66_3-018 airfoil at R_c=160,000 and α=12.0° show a local minimum in H_{32} at transition. This compares favorably with Fitzgerald transformed hot-wire data trends. Transformed hot-wire data is data that has been corrected for flow direction and it typically exhibited larger magnitude reverse flows than Fitzgerald's LDV data. Fitzgerald's LDV data shows a local minimum in H_{32} at transition. The transformed hot-wire data shows a local peak in H_{32} just after transition. Physically this indicates the energy dissipation to momentum loss ratio is large just after transition. The E387 measurements showed no discernable trend in H_{32} in the bubble but energy dissipation thickness did reach a peak at transition. The bubble examples in Table I all show a general increase in H_{12} in the bubble region except for the NACA 66_3-018 airfoil at R_c=160,000.

REFERENCES

Bogard, David G. and Tiederman, W. G. (1979): "Experimental Evaluation of Sampling Bias in Naturally Seeded Flows," *Laser Velocimetry and Particle Sizing*, edited by H. Doyle Thompson and Warren H. Stevenson, Hemisphere Publishing Corporation.

Brendel, M., and T. J. Mueller (1987): "Boundary Layer Measurements on an Airfoil at Low Reynolds Numbers," AIAA Paper 87-0495.

Drela, M. (1987): "Viscous-Inviscid Analysis of Transonic and Low Reynolds Number Airfoils," AIAA Journal, Vol. 25, No. 10, October.

Drela, M. (1989): "XFOIL: An Analysis and Design System for Low Reynolds Number Airfoils," Conference on Low Reynolds Number Aerodynamics, Preliminary Proceedings, Editor T.J. Mueller, June.

Eppler, R. (1986): "Recent Developments in Boundary Layer Computation, "Aerodynamics at Low Reynolds Numbers 10^4 <Re<10^6 International Conference", Vol. II Proceedings, October, pp. 12.1-12.18.

Fitzgerald, E. J. (1988): "Experimental Studies of the Transitional Separation Bubble on the NACA 66_3-018 Airfoil at Low Reynolds Numbers," M.S. Thesis, University of Notre Dame.

McGhee, Robert J. , Betty S. Walker, and Betty F. Millard (1988): Experimental Results for the Eppler 387 Airfoil at Low Reynolds Numbers in the Langley Low-Turbulence Pressure Tunnel," NASA Technical Memorandum 4062, October.

Meyers, James F. (1979): "Applications of Laser Velocimetry To Large Scale and Specialized Aerodynamic Tests," TSI Quarterly, Vol. V, Issue 4, December.

TABLE I

SEPARATION BUBBLE PARAMETERS

From LDV Data Except as Indicated

Airfoil	E387	FX63-137 (hot-wire)	FX63-137	FX63-137 (lower surface)	NACA 66_3-018	NACA 66_3-018
angle of attack	2.0°	3.0°	7.0°	-5.0°	12.0°	12.0°
R_c (x 10^{-5})	1.0	1.0	1.0	1.0	1.4	1.6
S (%chord)	39.5	42	33	2	1.2	3.0
T (% chord)	76	69	53	10	7.0	6.0
R (% chord)	80.5	80	59	†	12	9.0
chord (mm)	304.8	305	305	305	249.5	249.5
l_1 (mm)	111.3	83	61	25	2.48	1.94
AR_b	33.0	15.4	20.3	9.6	5.8	3.2
γ	2.6°	3.7°	2.8°	7.0°	9.6°	16.3°
Rl_1 (x10^{-3})	32.5	41	31	12	16.1	9.4
$R_{\delta_{1s}}$	670	609	597	191	654	488
$R_{\delta_{2s}}$	160.6	194	180	57	100.7	75
$R_{\delta_{1t}}$	1990	3084	2136	1422	3408	3375
$R_{\delta_{2t}}$	119	503	345	71	271	125
δ_{1s} (mm)	1.65	1.2	1.2	0.4	0.589	0.39
δ_{1t} (mm)	2.41	6.6	4.2	3.0	3.07	2.7
δ_{2s} (mm)	0.404	0.40	0.36	0.12	0.09	0.06
δ_{2t} (mm)	1.26	1.07	0.68	0.15	0.244	-0.10
H_{12s}	4.07	3.15	3.33	3.33	6.72	2.6
H_{12t}	1.91	6.13	6.21	20	12.51	-25.9
H_{32s}	1.63	1.54	1.56	1.5	1.43	1.5
H_{32t}	1.74	1.37	1.49	1.82	1.74	-0.41
U_∞ (m/sec)	5.3	†	†	†	9.9	10.3
U_{e_s} (m/sec)	6.4	†	†	†	17.8	20.0

† indicates no table entry

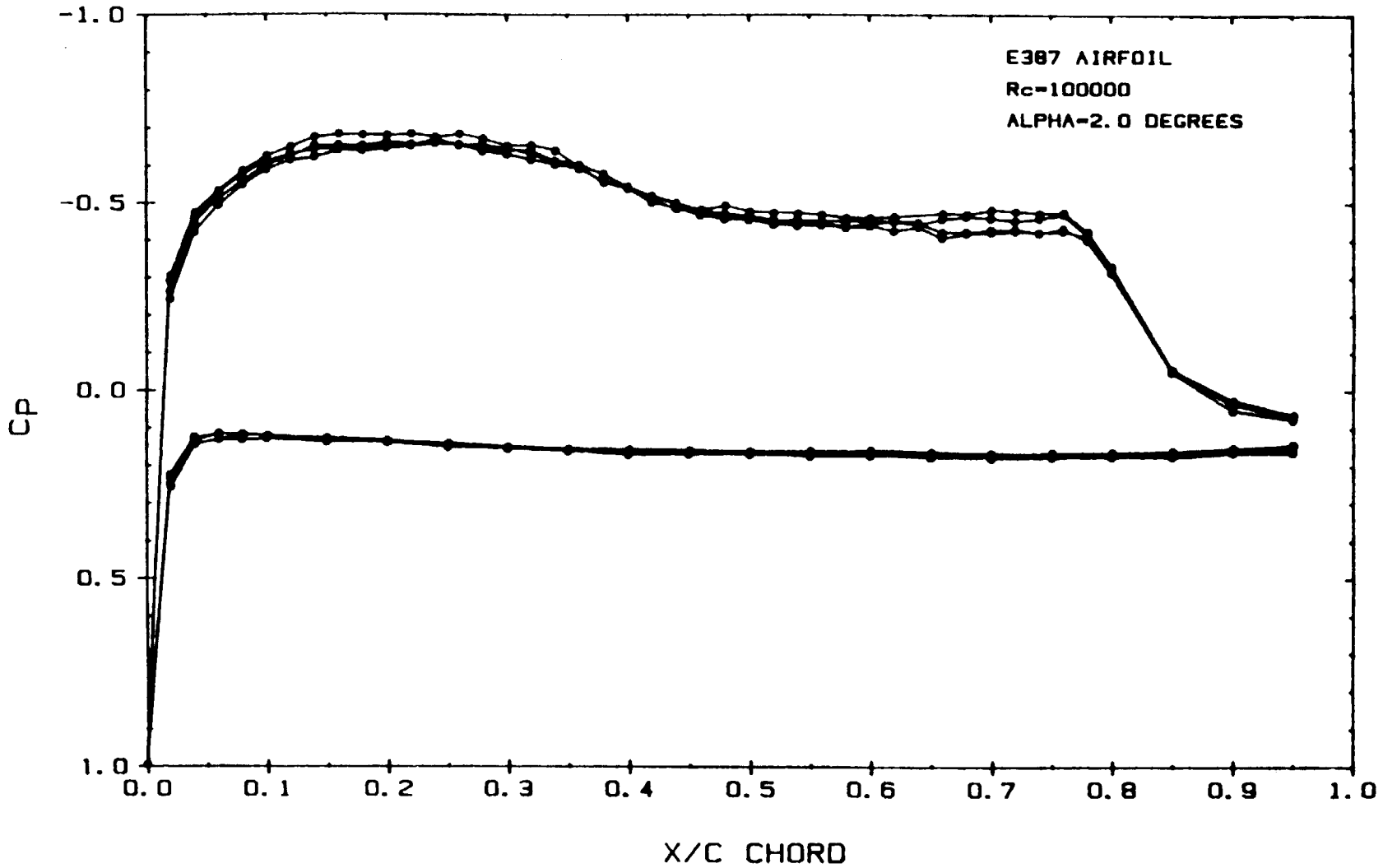

Figure 1 Static Pressure Measurement Repeatability for E387 Airfoil at R_c = 100,000 and α = 2.0°

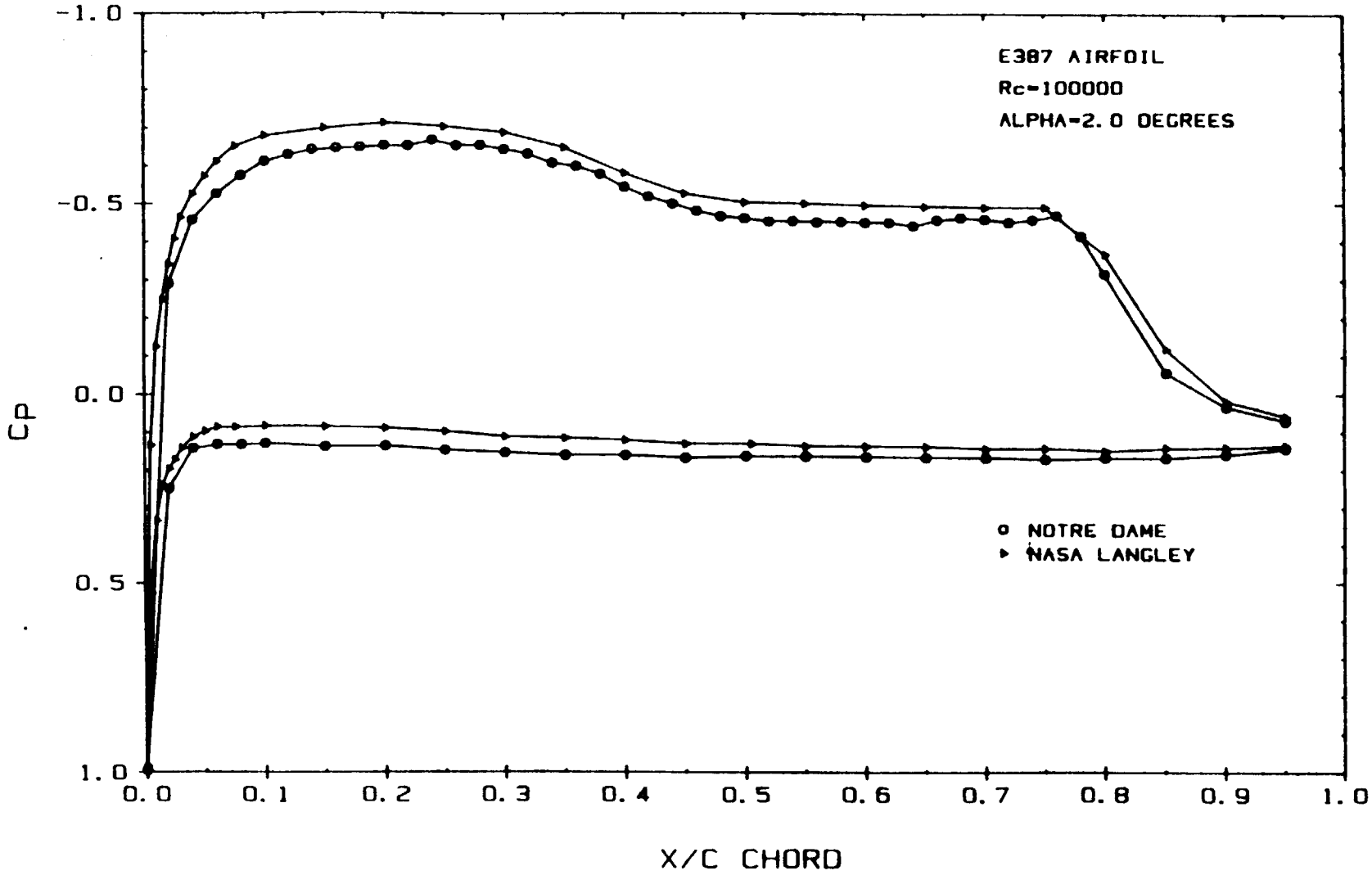

Figure 2 Static Pressure Measurement Comparison for Notre Dame and NASA Langley Tests of E387 Airfoil at R_c =100,000 and α = 2.0°

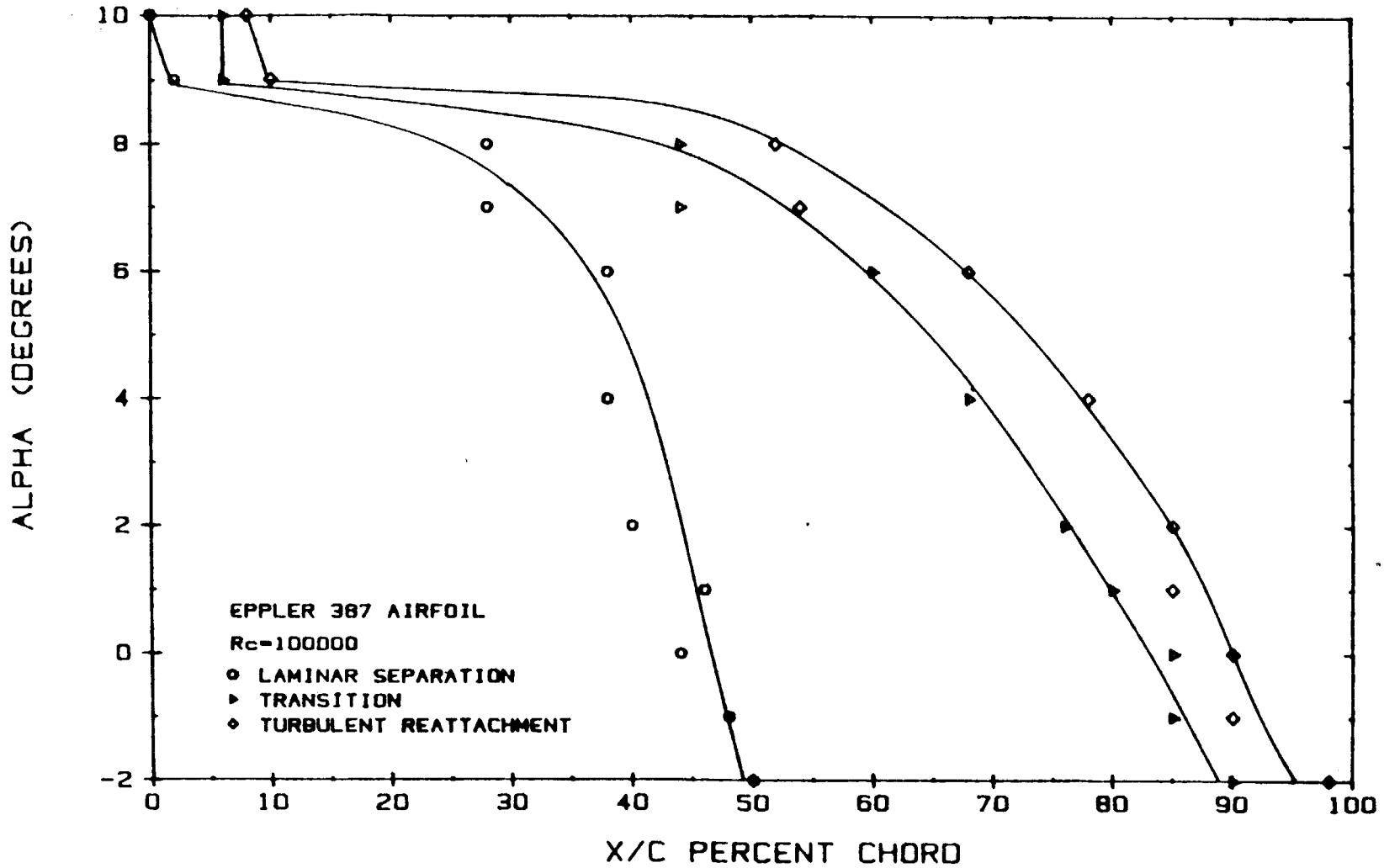

Figure 3 Summary of Laminar Separation, Transition, and Turbulent Reattachment Locations for Various Angles of Attack for the E387 Airfoil at R_c = 100,000

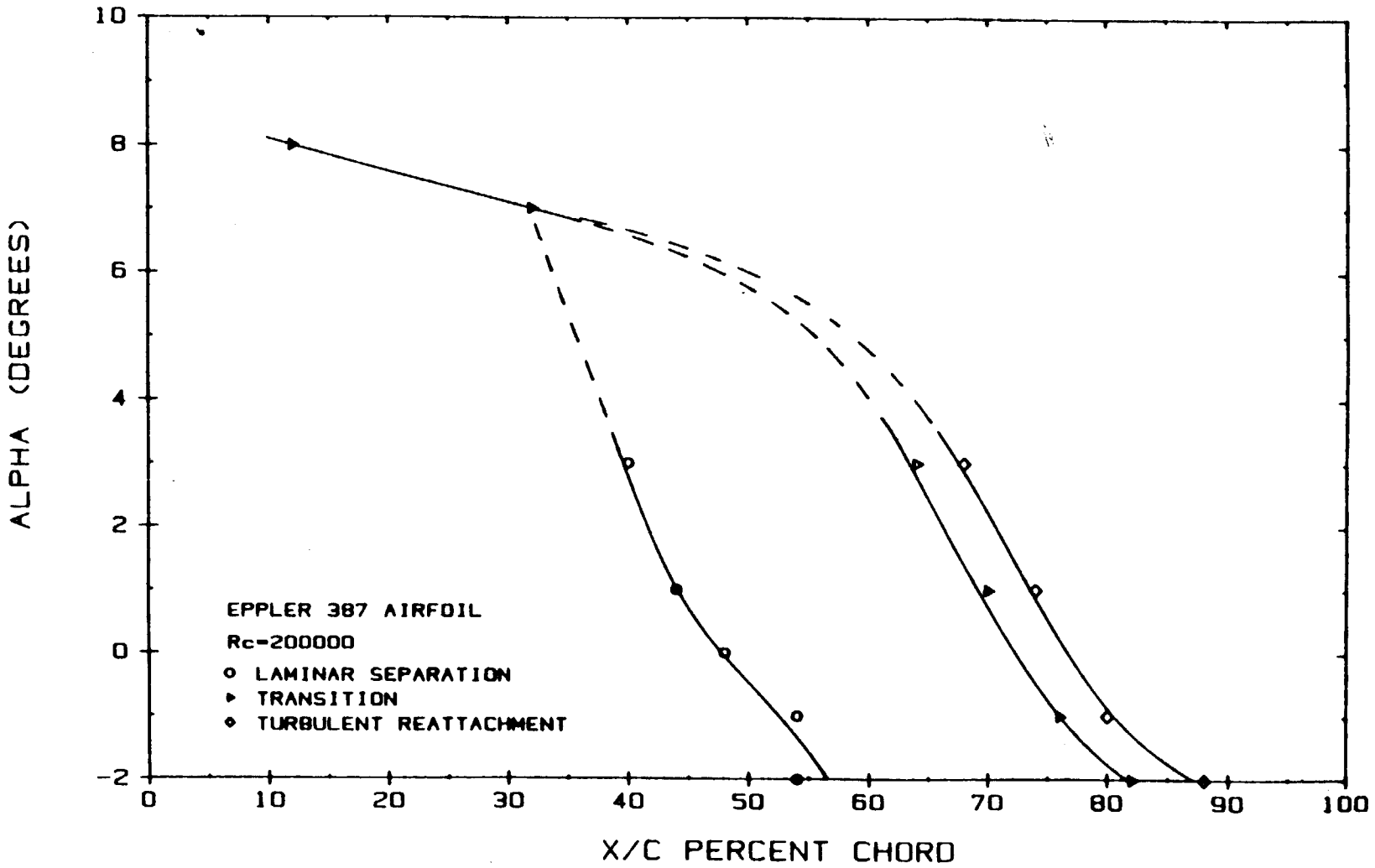

Figure 4 Summary of Laminar Separation, Transition, and Turbulent Reattachment Locations for Various Angles of Attack for the E387 Airfoil at R_c = 200,000

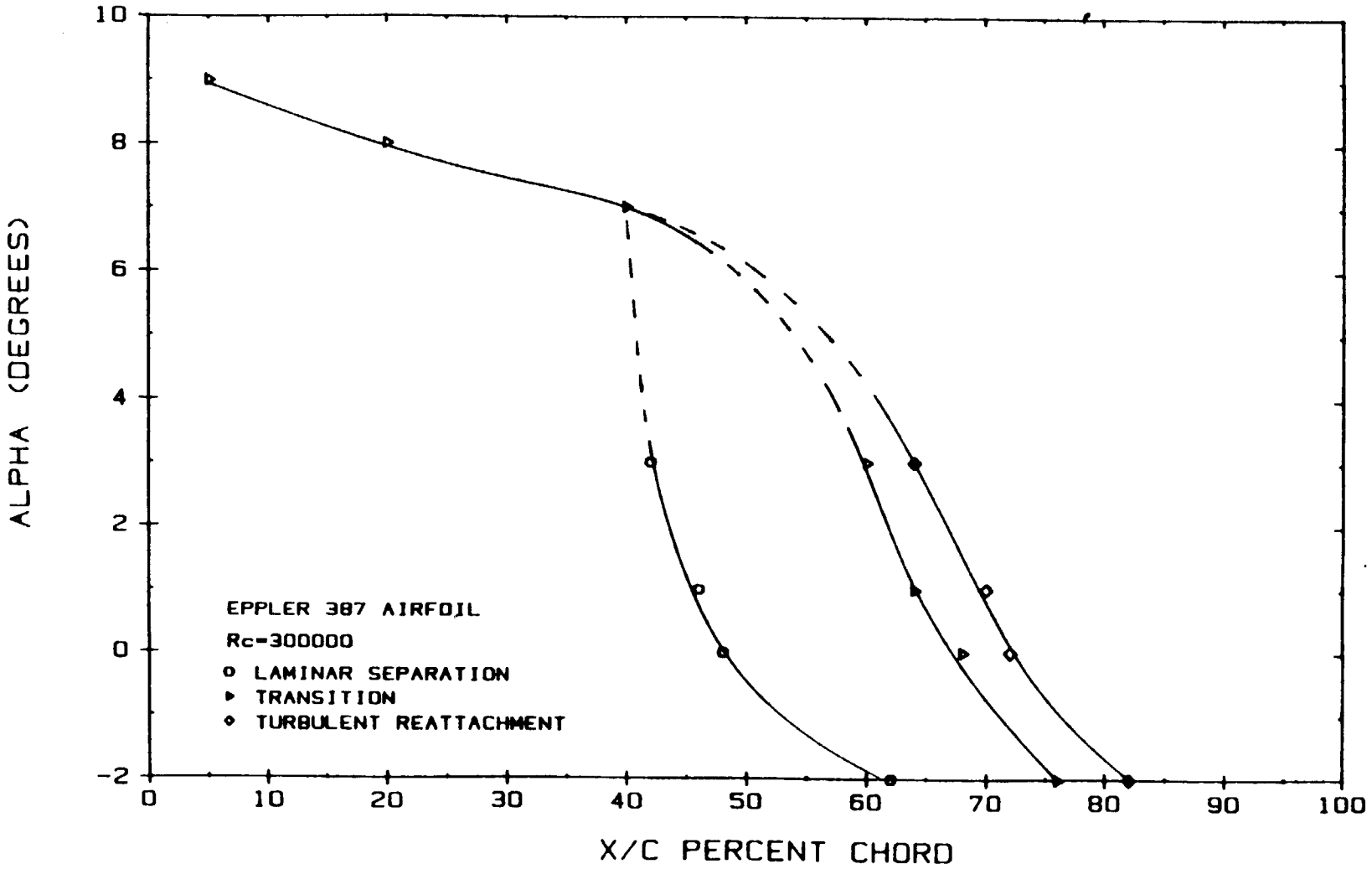

Figure 5 Summary of Laminar Separation, Transition, and Turbulent Reattachment Locations for Various Angles of Attack for the E387 Airfoil at $R_c = 300,000$

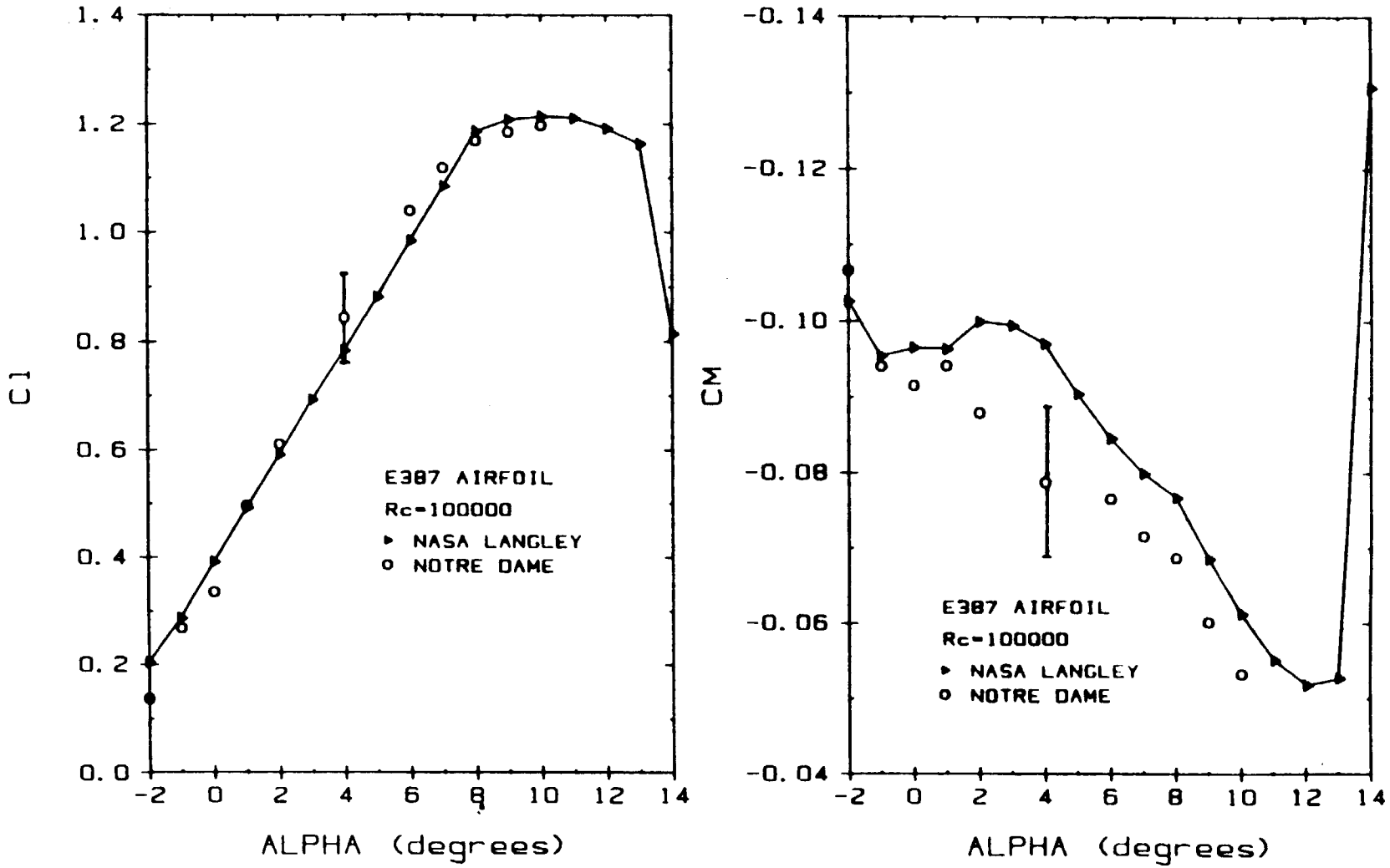

Figure 6 Comparison of Notre Dame and NASA Langley Lift and Moment Curves for the E387 Airfoil at R_c = 100,000

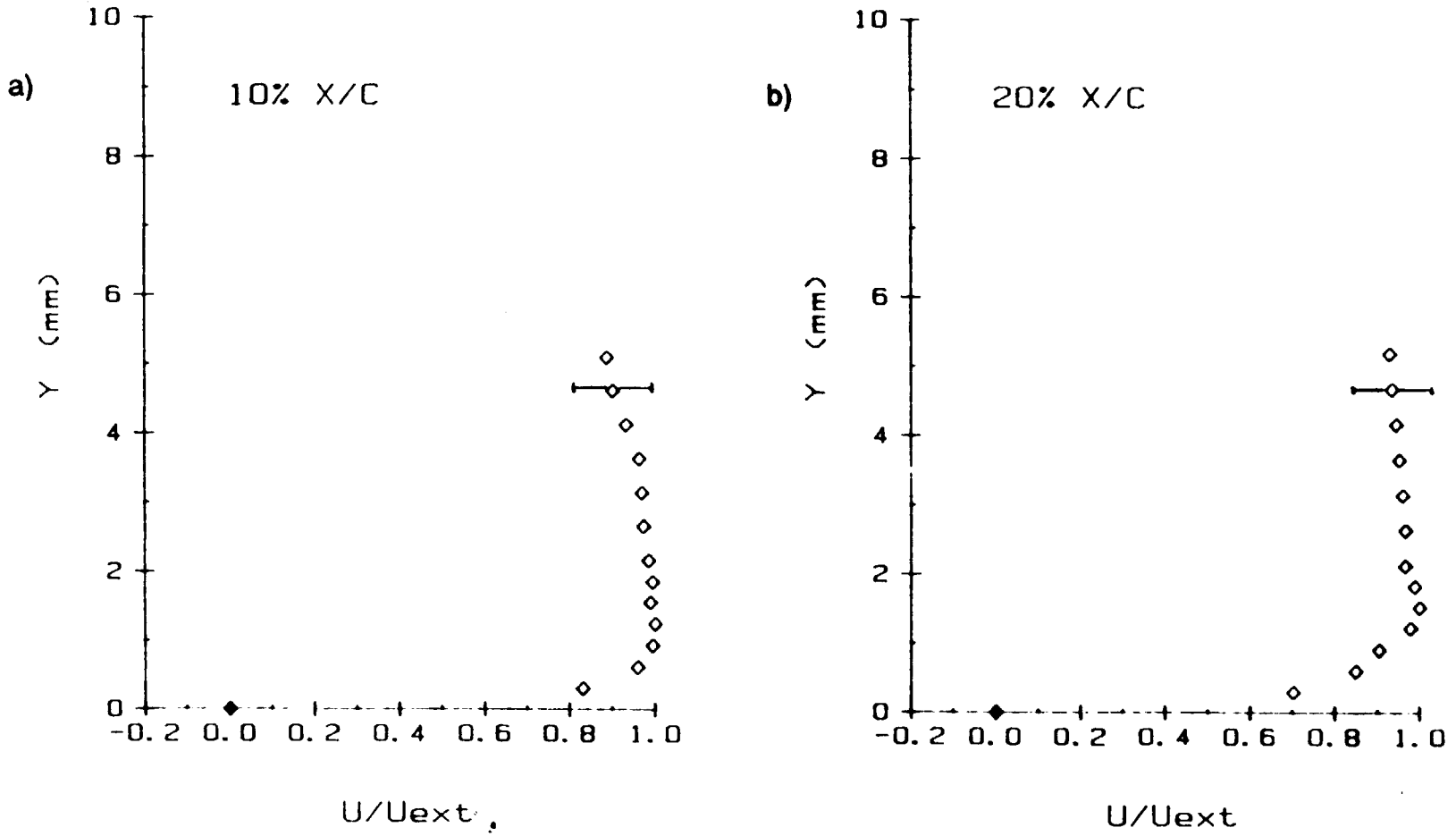

Figure 7 E387 Airfoil LDV U/U_{ext} Boundary Layer Velocity Profiles, 10% x/c and 20% x/c Chord Positions, $R_c = 100{,}000$, $\alpha = 2.0°$

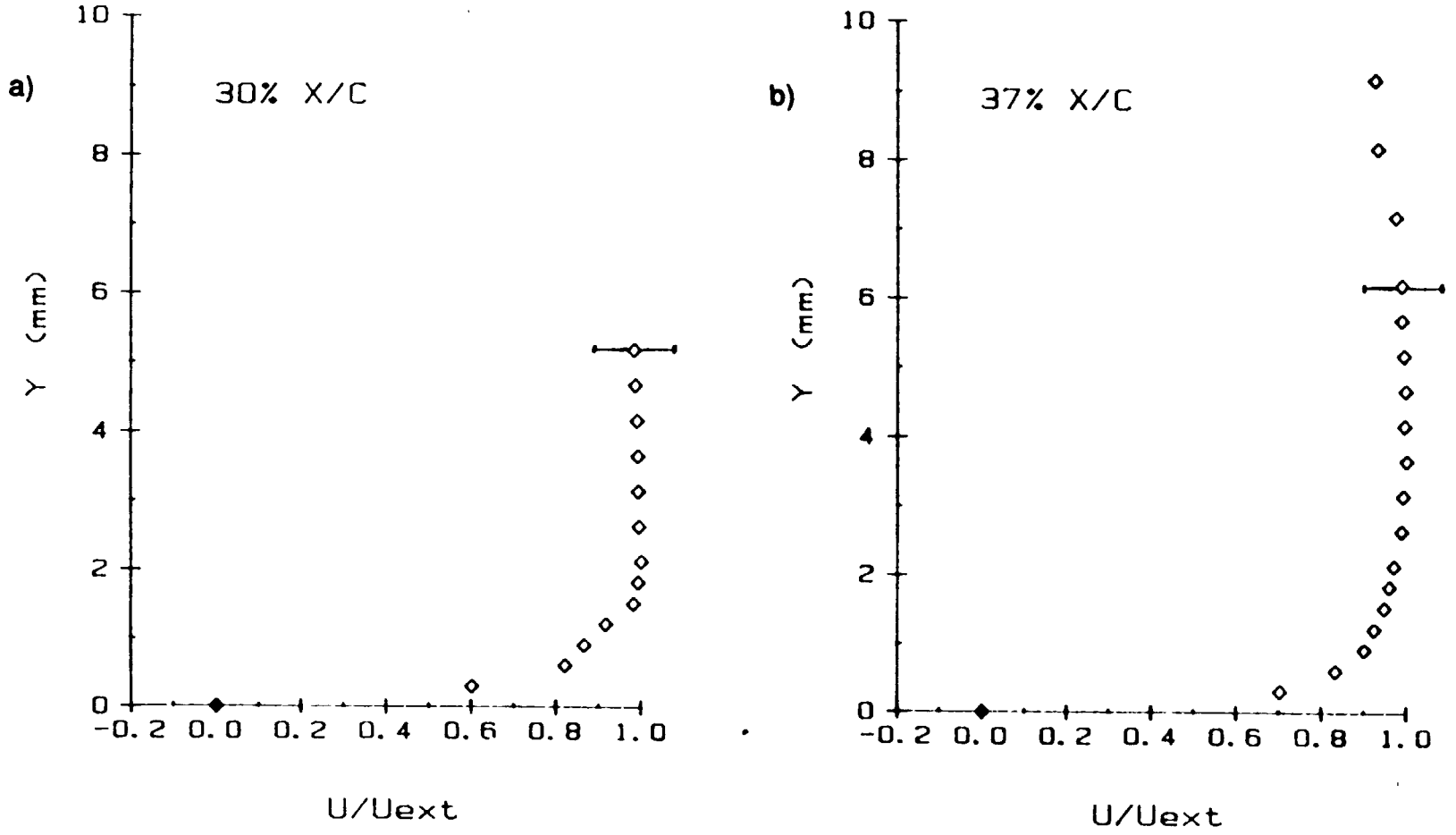

Figure 8 **E387 Airfoil LDV U/U_{ext} Boundary Layer Velocity Profiles, 30% x/c and 37% x/c Chord Positions, R_c = 100,000 , α = 2.0°**

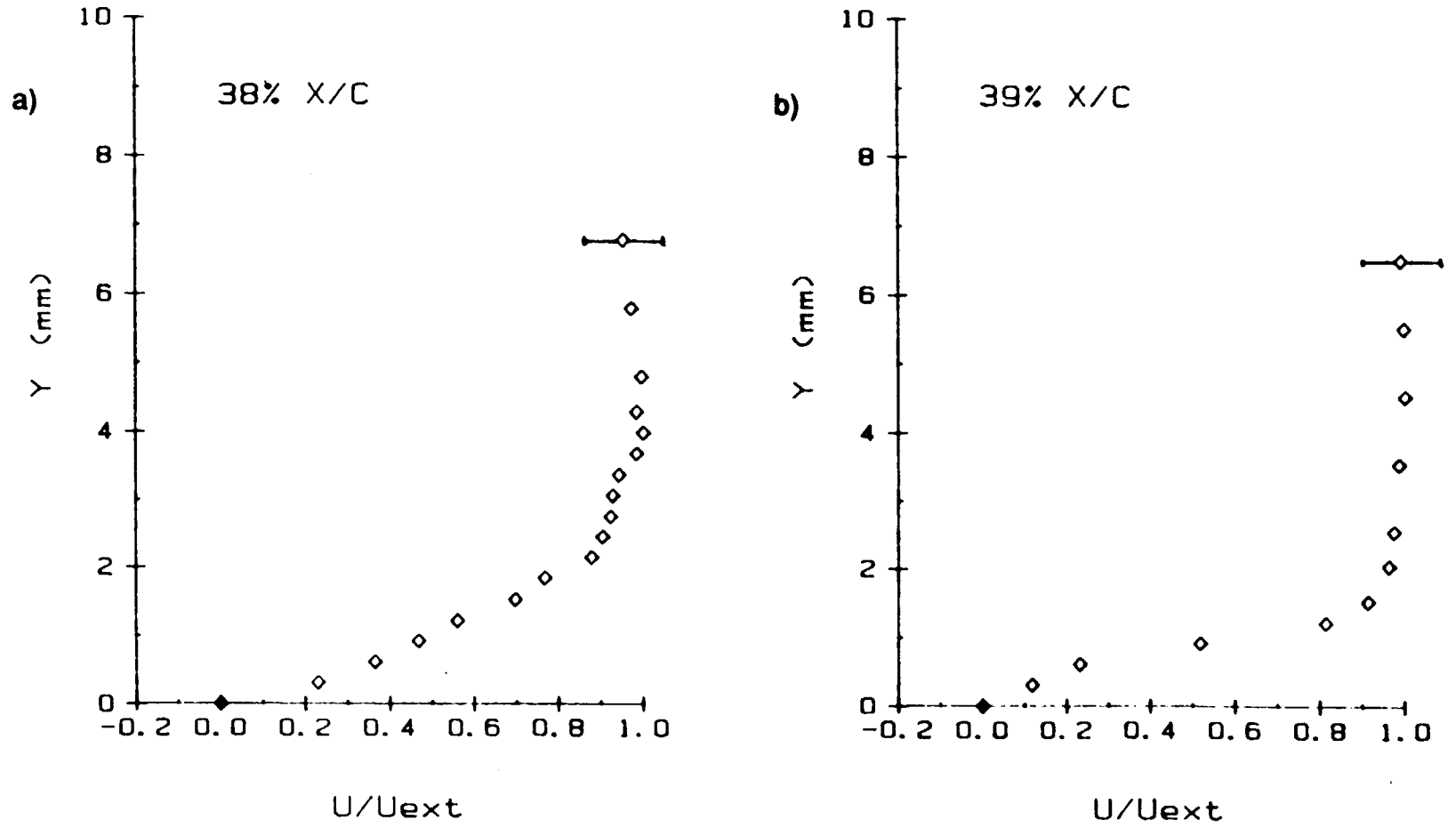

Figure 9 **E387 Airfoil LDV U/U_{ext} Boundary Layer Velocity Profiles, 38% x/c and 39% x/c Chord Positions, R_c = 100,000 , α = 2.0°**

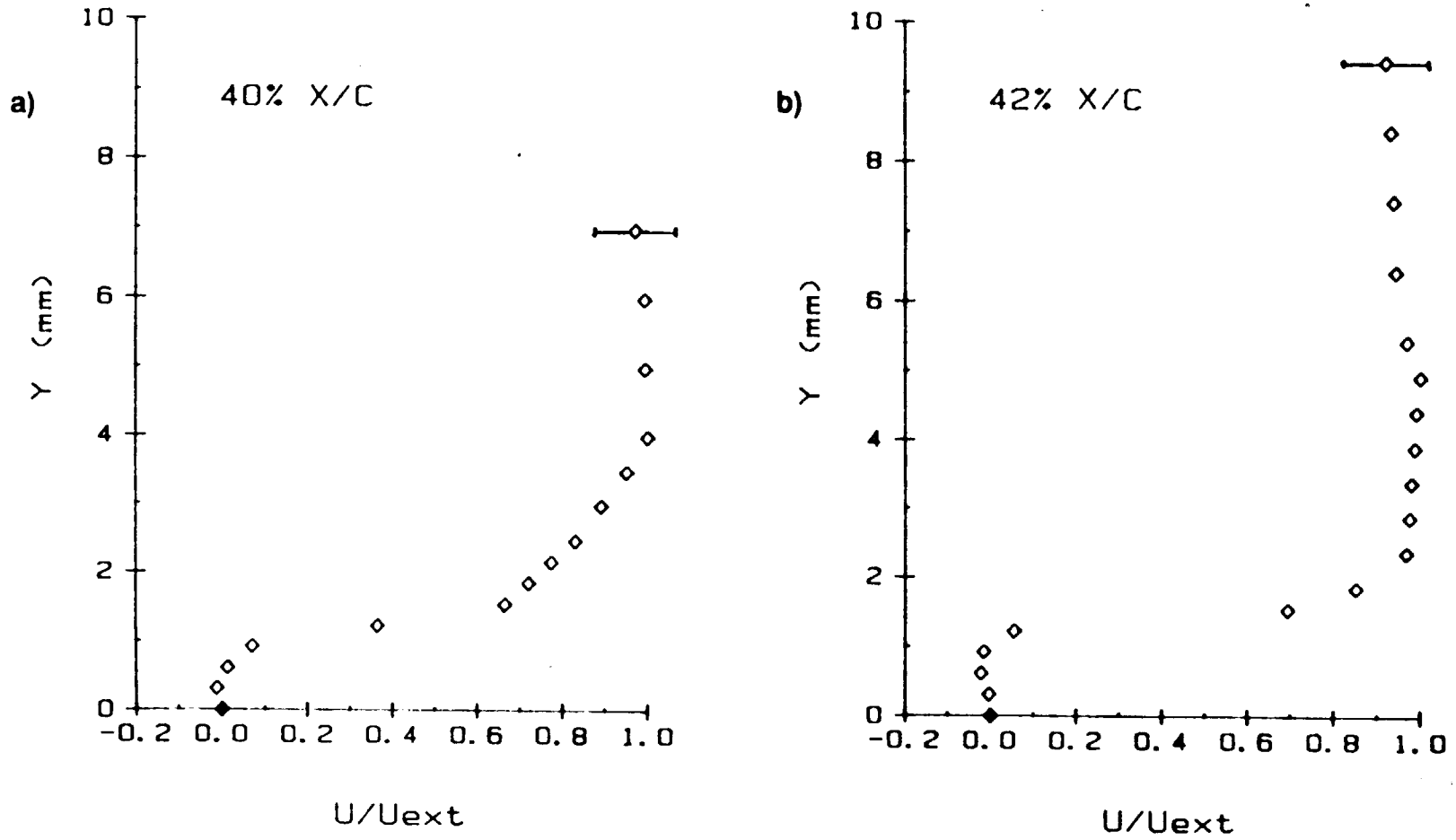

Figure 10 **E387 Airfoil LDV U/U_{ext} Boundary Layer Velocity Profiles, 40% x/c and 42% x/c Chord Positions, R_c = 100,000 , α = 2.0°**

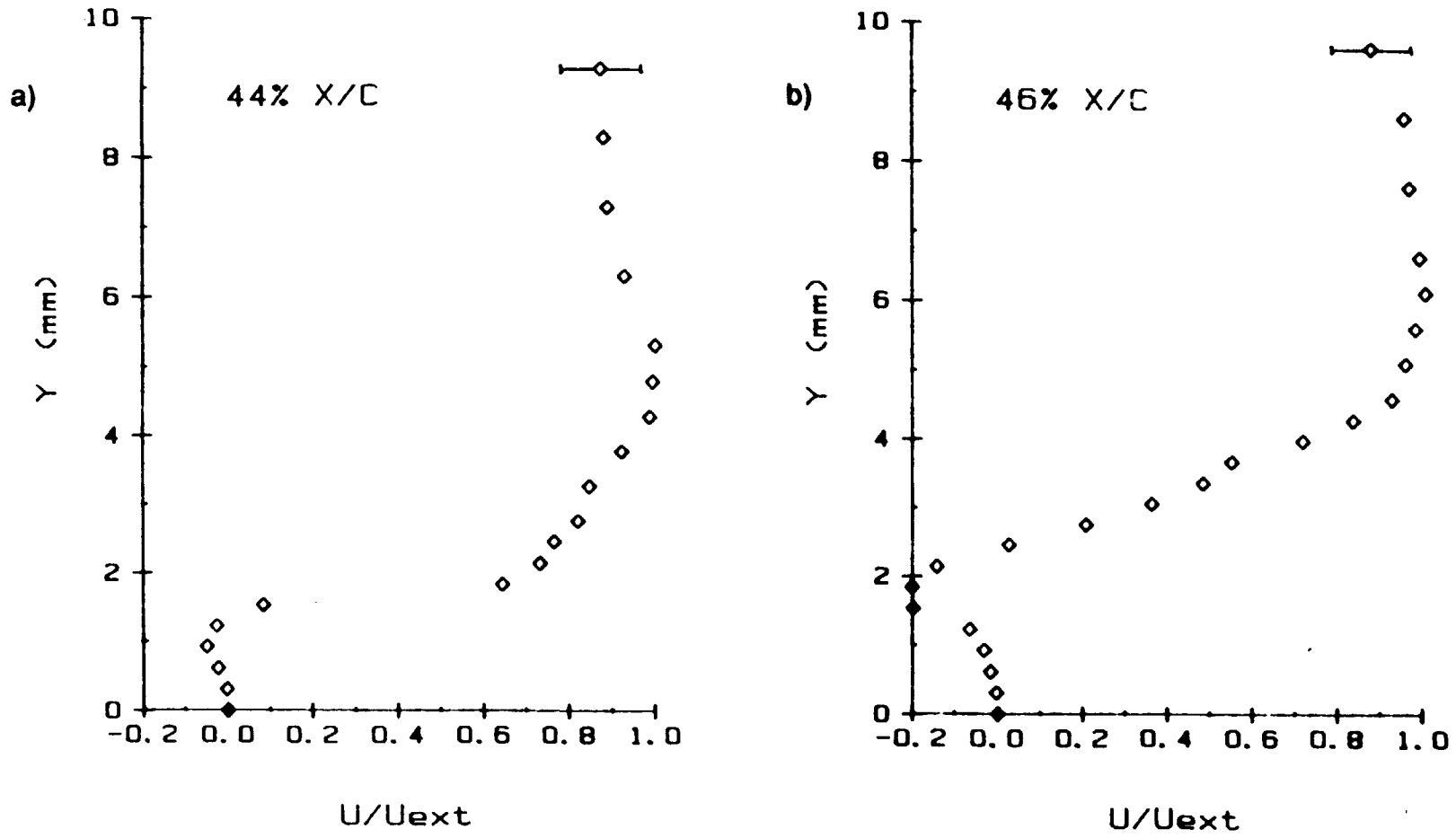

Figure 11 E387 Airfoil LDV U/U_{ext} Boundary Layer Velocity Profiles, 44% x/c and 46% x/c Chord Positions, R_c = 100,000 , α = 2.0°

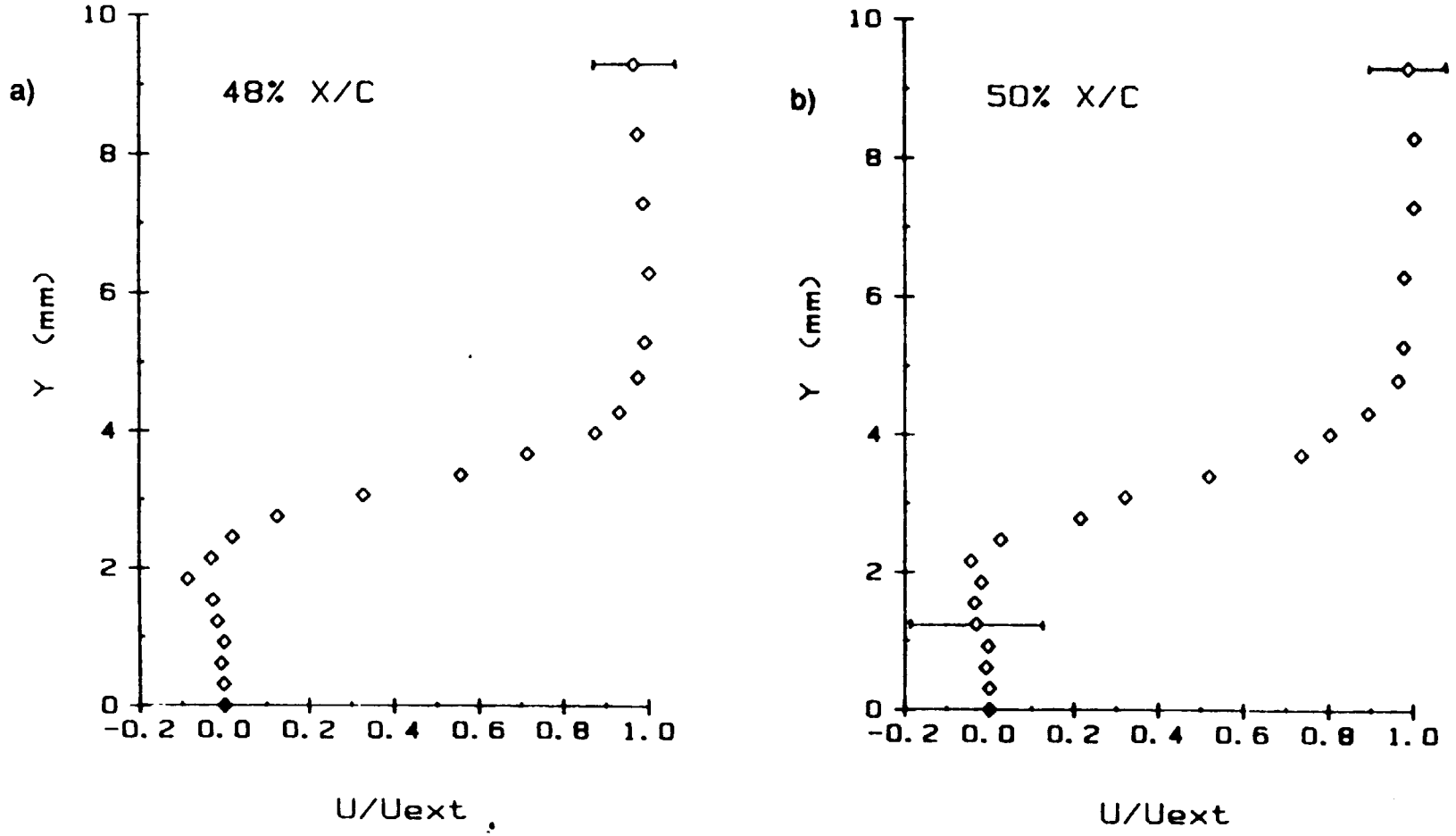

Figure 12 E387 Airfoil LDV U/U_{ext} Boundary Layer Velocity Profiles, 48% x/c and 50% x/c Chord Positions, $R_c = 100{,}000$, $\alpha = 2.0°$

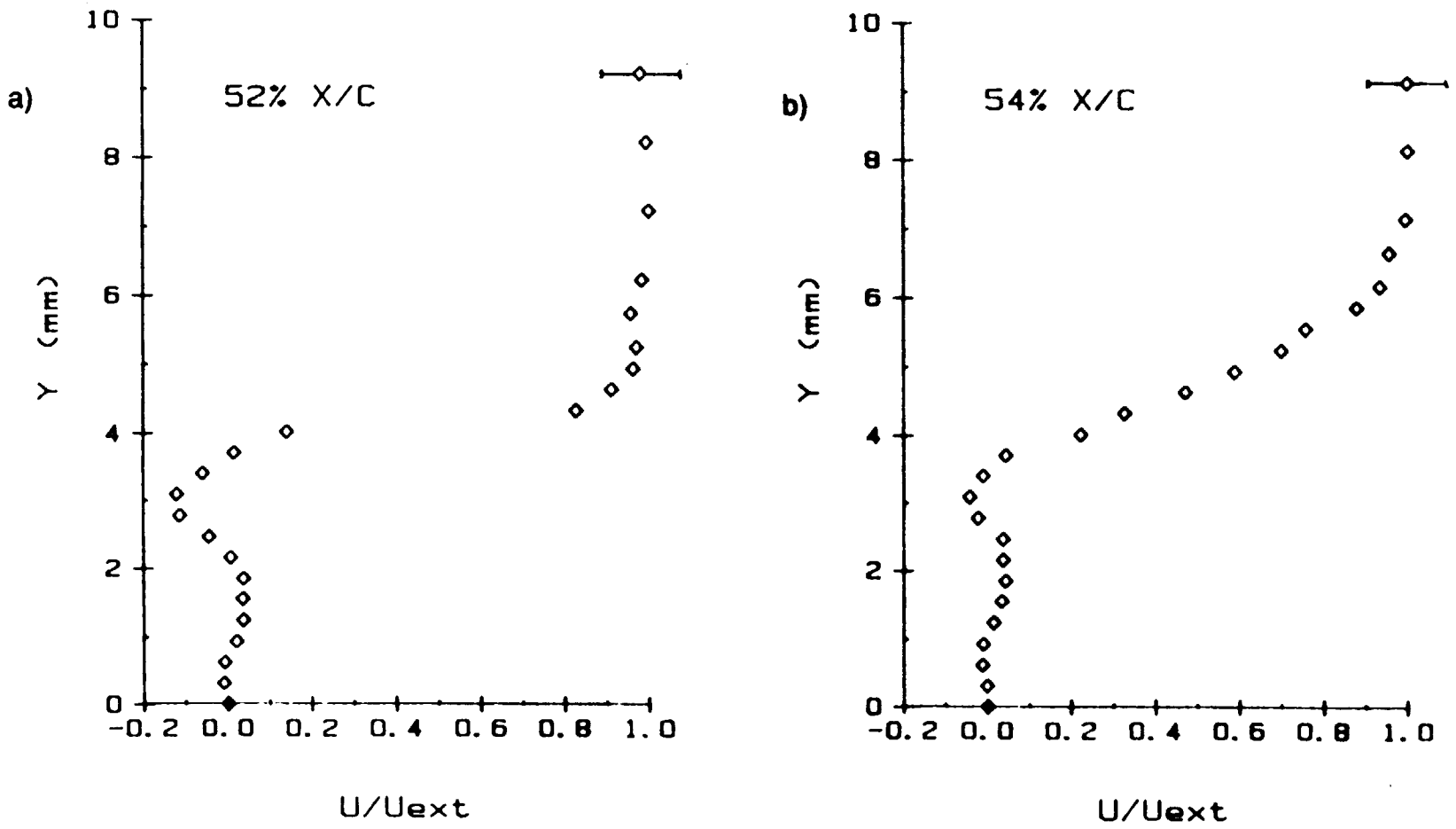

Figure 13 **E387 Airfoil LDV U/U_{ext} Boundary Layer Velocity Profiles, 52% x/c and 54% x/c Chord Positions, R_c = 100,000 , α = 2.0°**

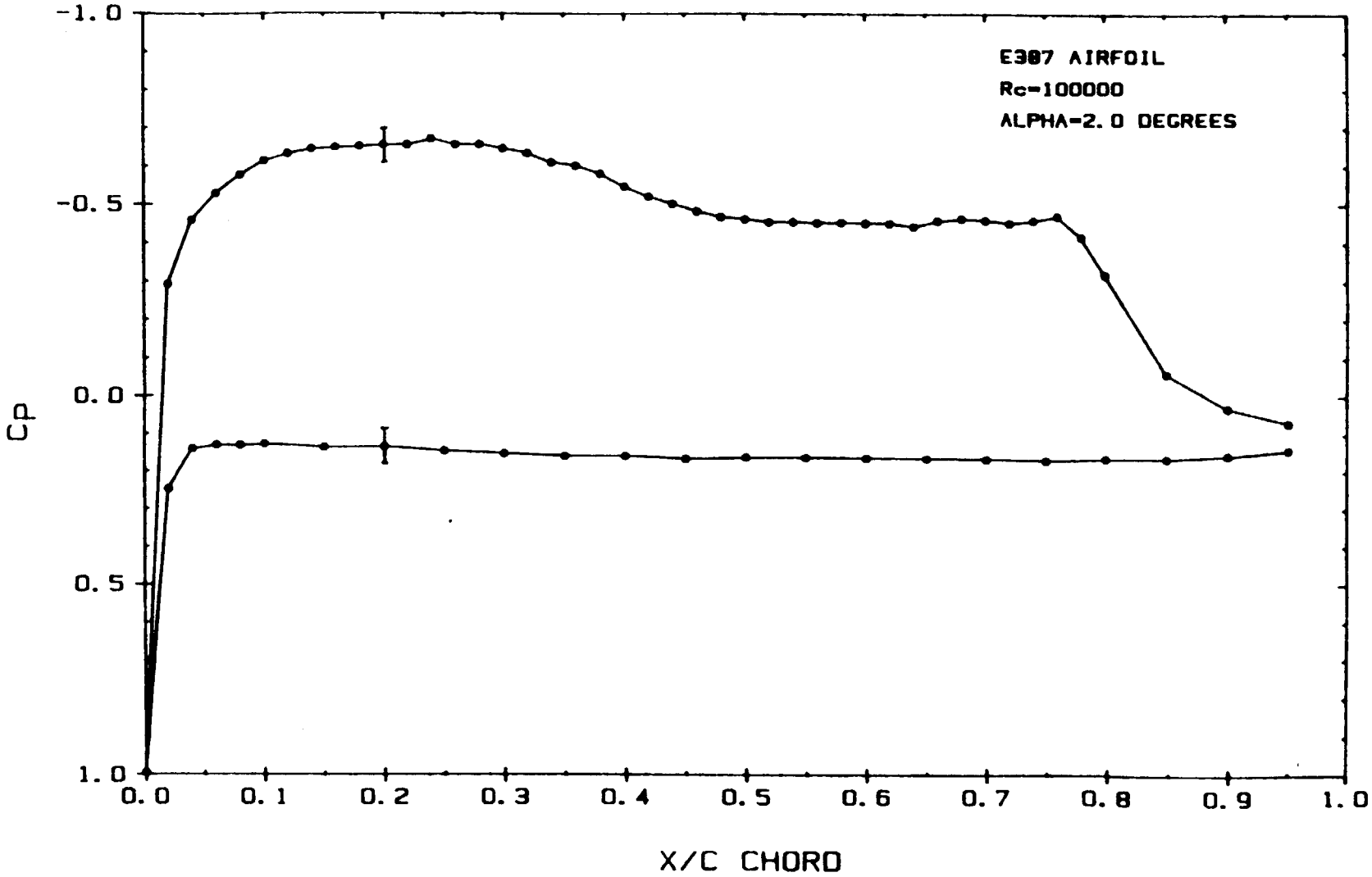

Figure 14 Static Pressure Distribution for E387 Airfoil
R_c = 100,000 , α = 2.0°

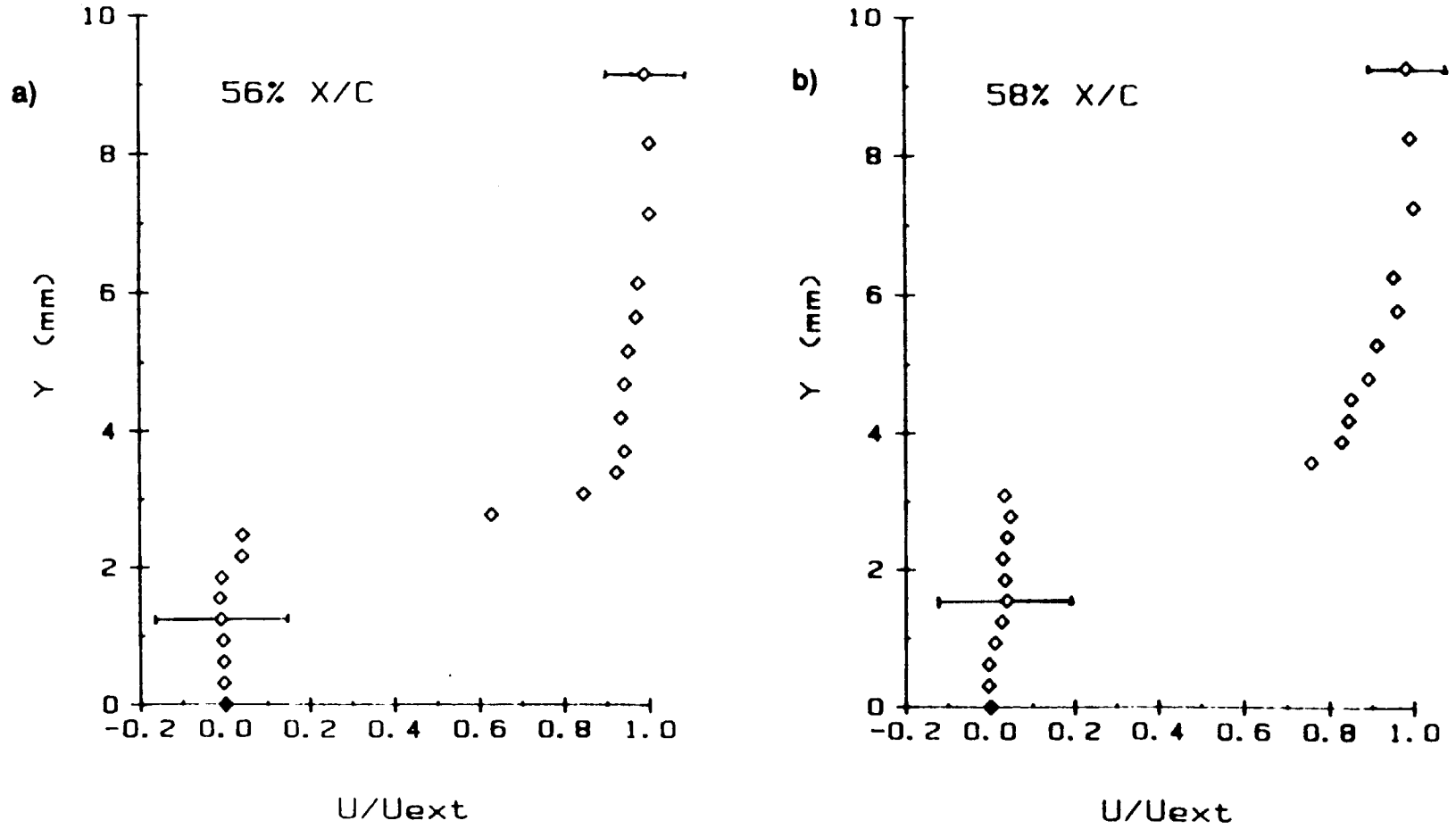

Figure 15 **E387 Airfoil LDV U/U_{ext} Boundary Layer Velocity Profiles, 56% x/c and 58% x/c Chord Positions, R_c = 100,000 , α = 2.0°**

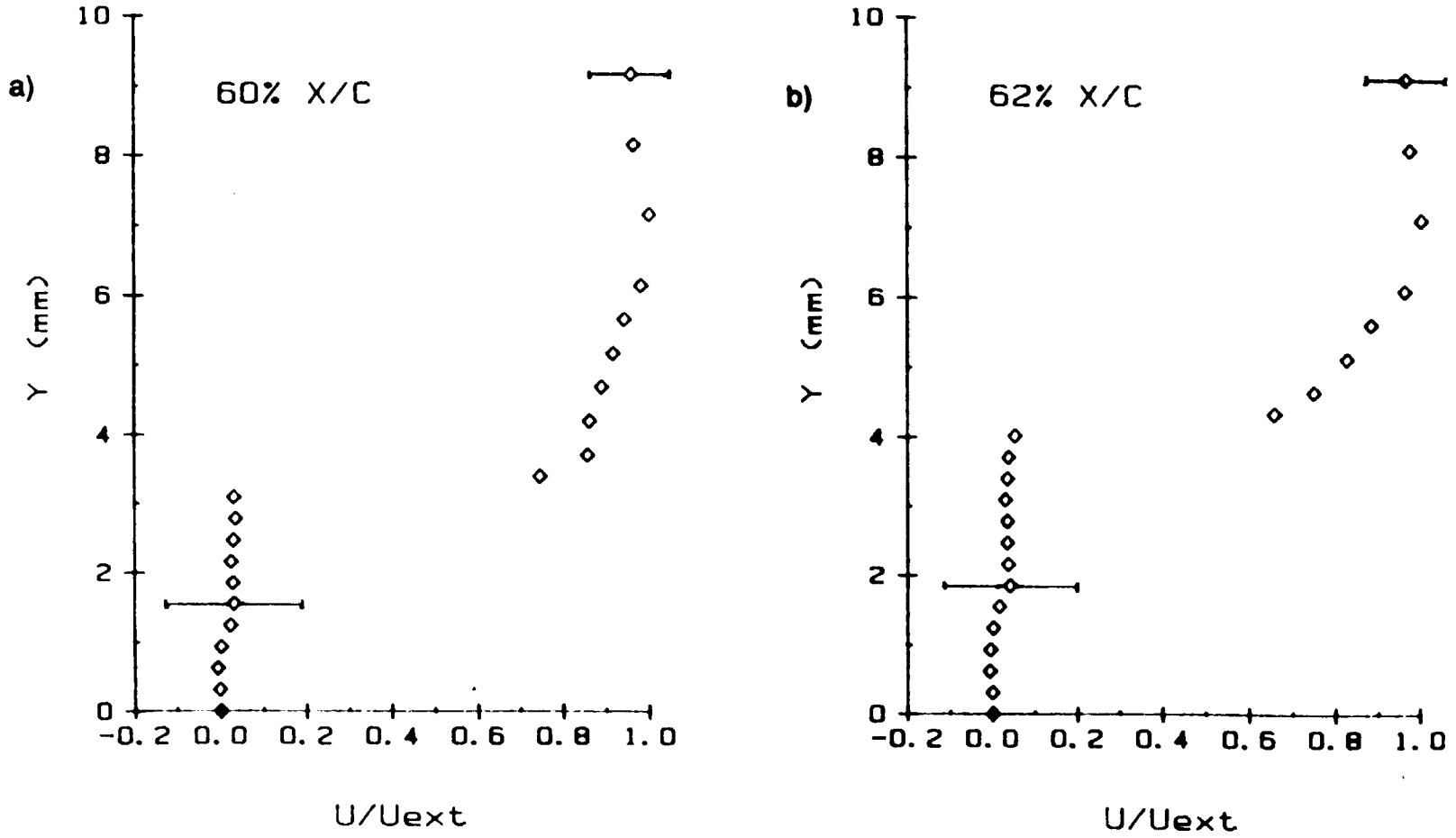

Figure 16 E387 Airfoil LDV U/U_{ext} Boundary Layer Velocity Profiles, 60% x/c and 62% x/c Chord Positions, $R_c = 100{,}000$, $\alpha = 2.0°$

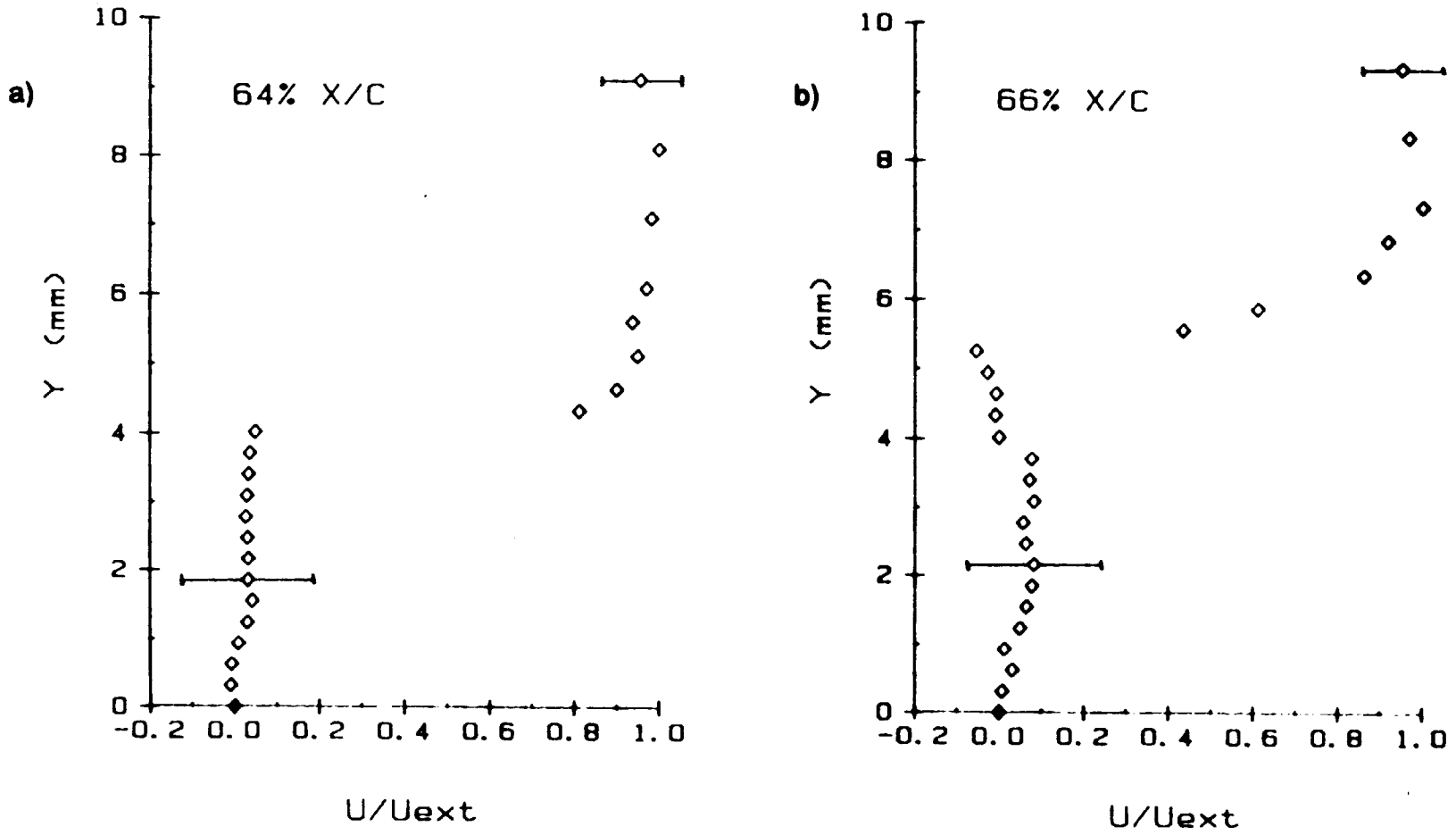

Figure 17 **E387 Airfoil LDV U/U_{ext} Boundary Layer Velocity Profiles, 64% x/c and 66% x/c Chord Positions, R_c = 100,000 , α = 2.0°**

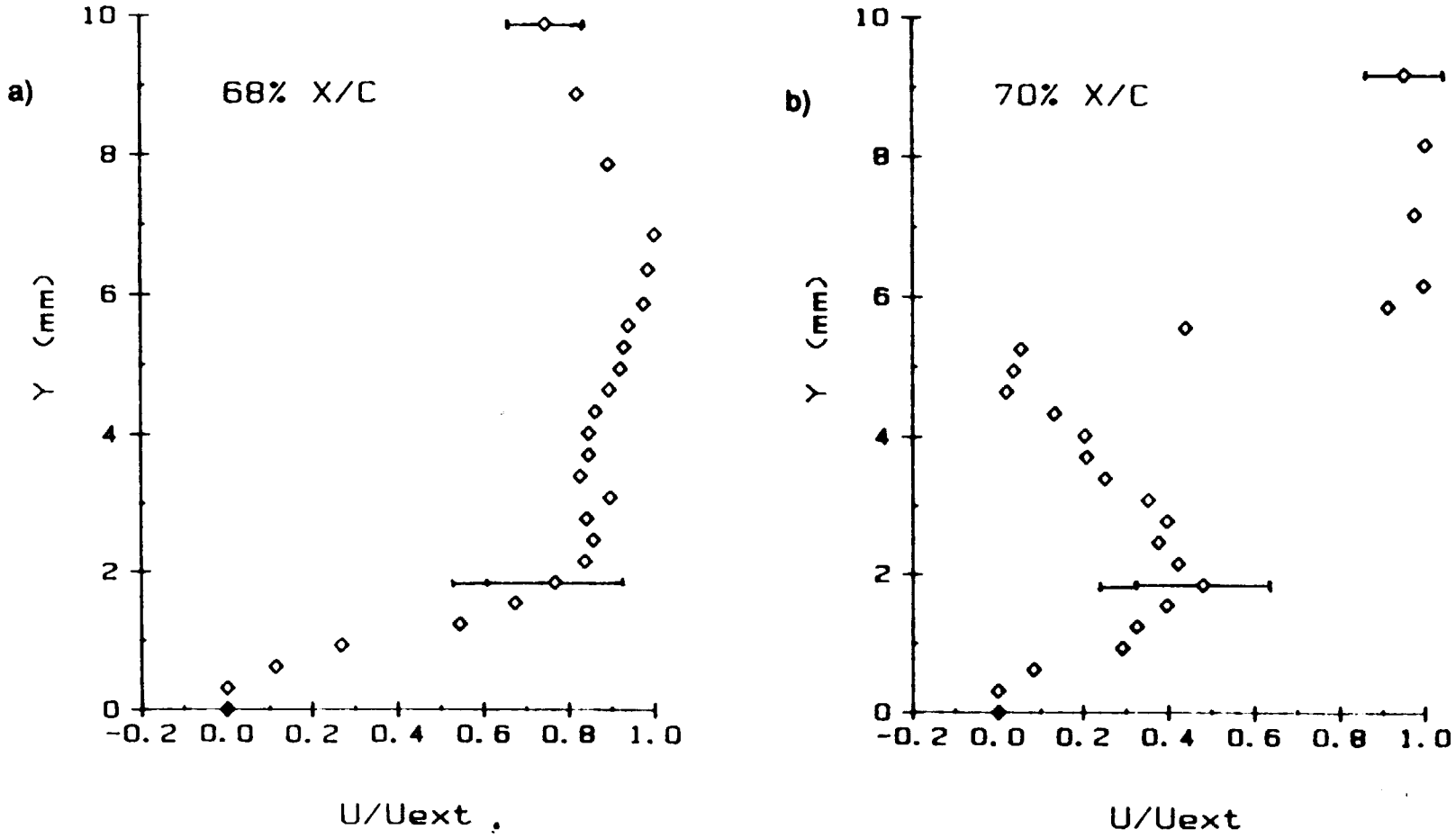

Figure 18 **E387 Airfoil LDV U/U_{ext} Boundary Layer Velocity Profiles, 68% x/c and 70% x/c Chord Positions, R_c = 100,000 , α = 2.0°**

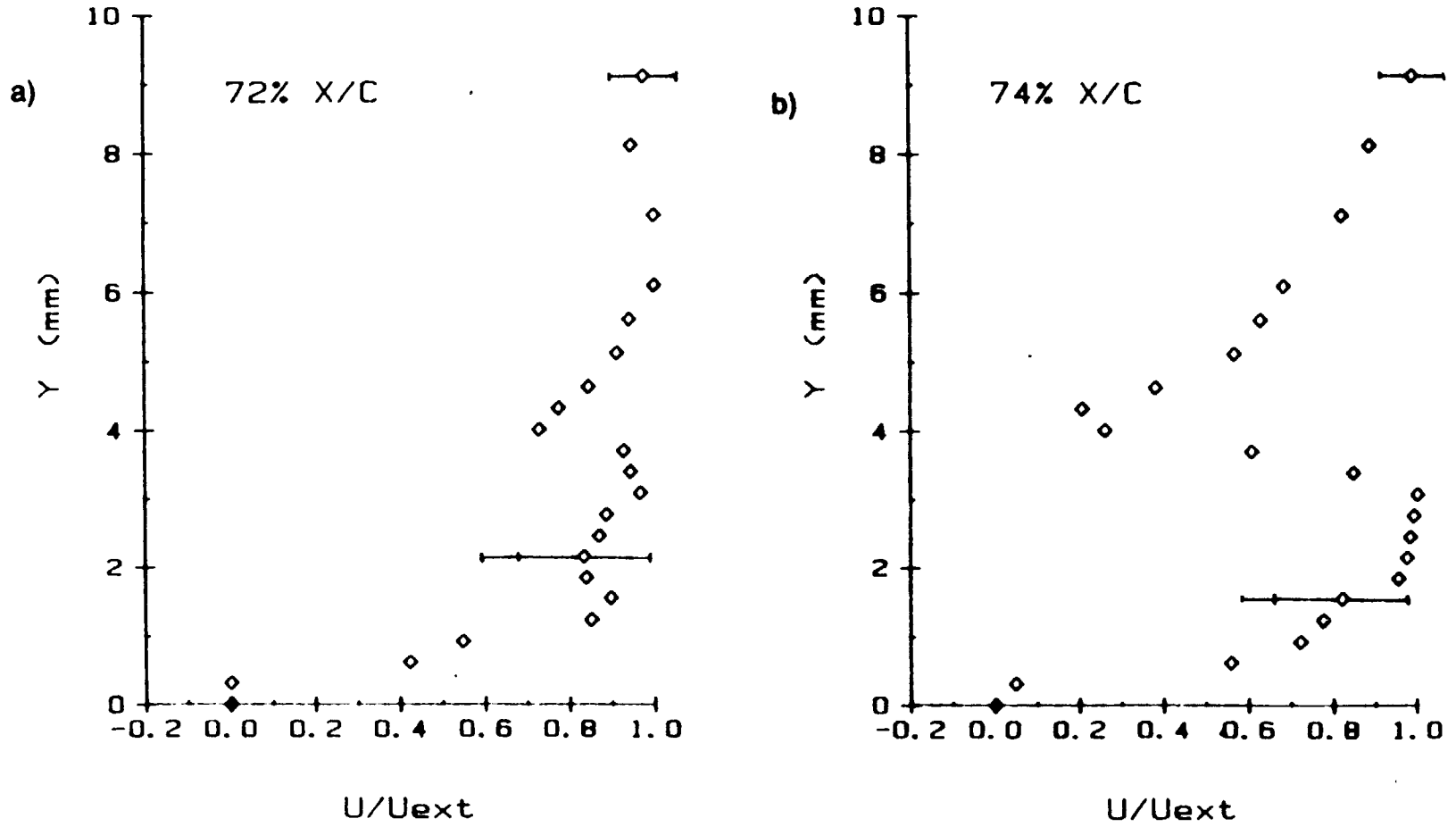

Figure 19 E387 Airfoil LDV U/U_{ext} Boundary Layer Velocity Profiles, 72% x/c and 74% x/c Chord Positions, R_c = 100,000 , α = 2.0°

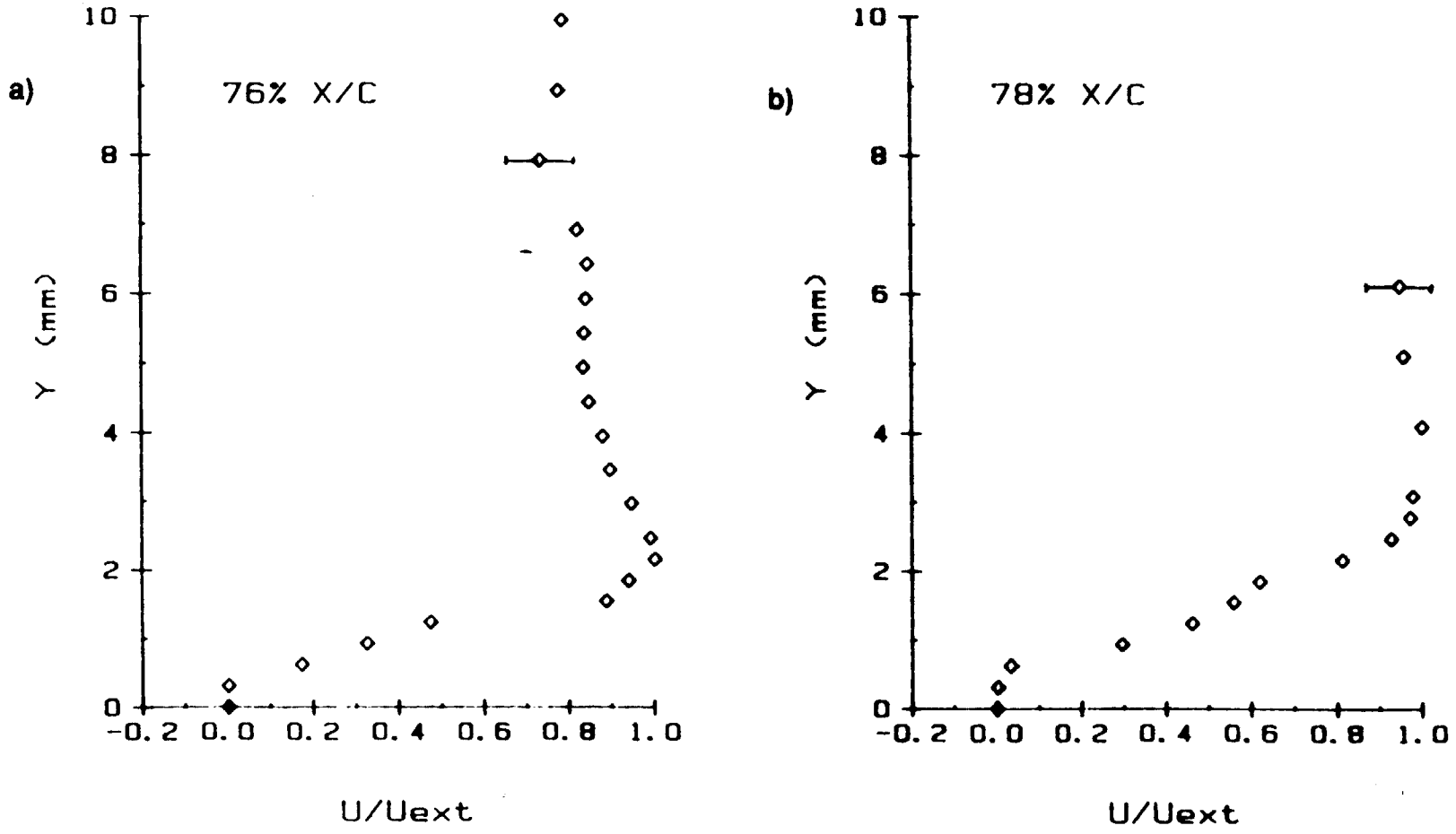

Figure 20 **E387 Airfoil LDV U/U_{ext} Boundary Layer Velocity Profiles, 76% x/c and 78% x/c Chord Positions, R_c = 100,000 , α = 2.0°**

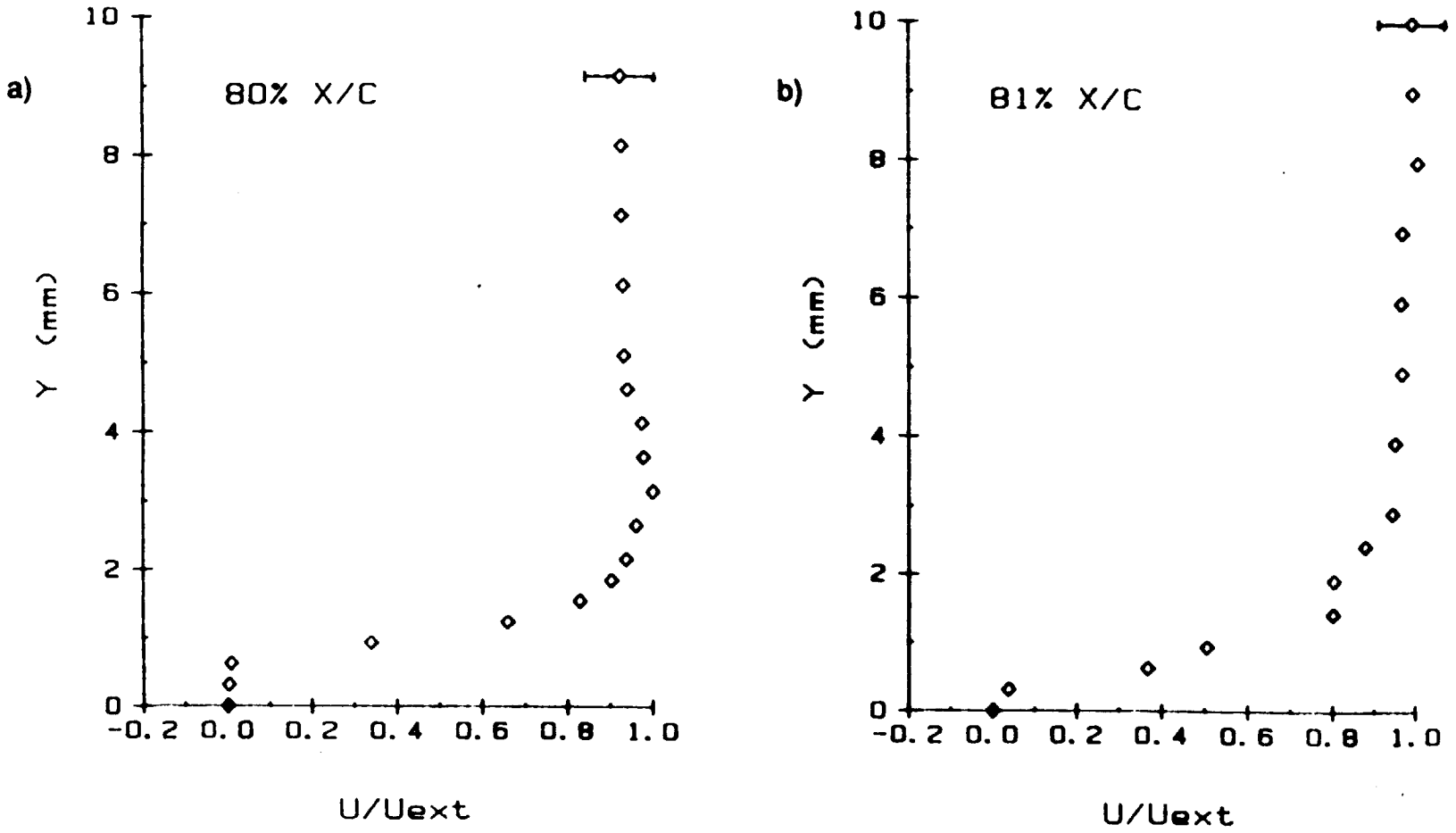

Figure 21 E387 Airfoil LDV U/U_{ext} Boundary Layer Velocity Profiles, 80% x/c and 81% x/c Chord Positions, R_c = 100,000 , α = 2.0°

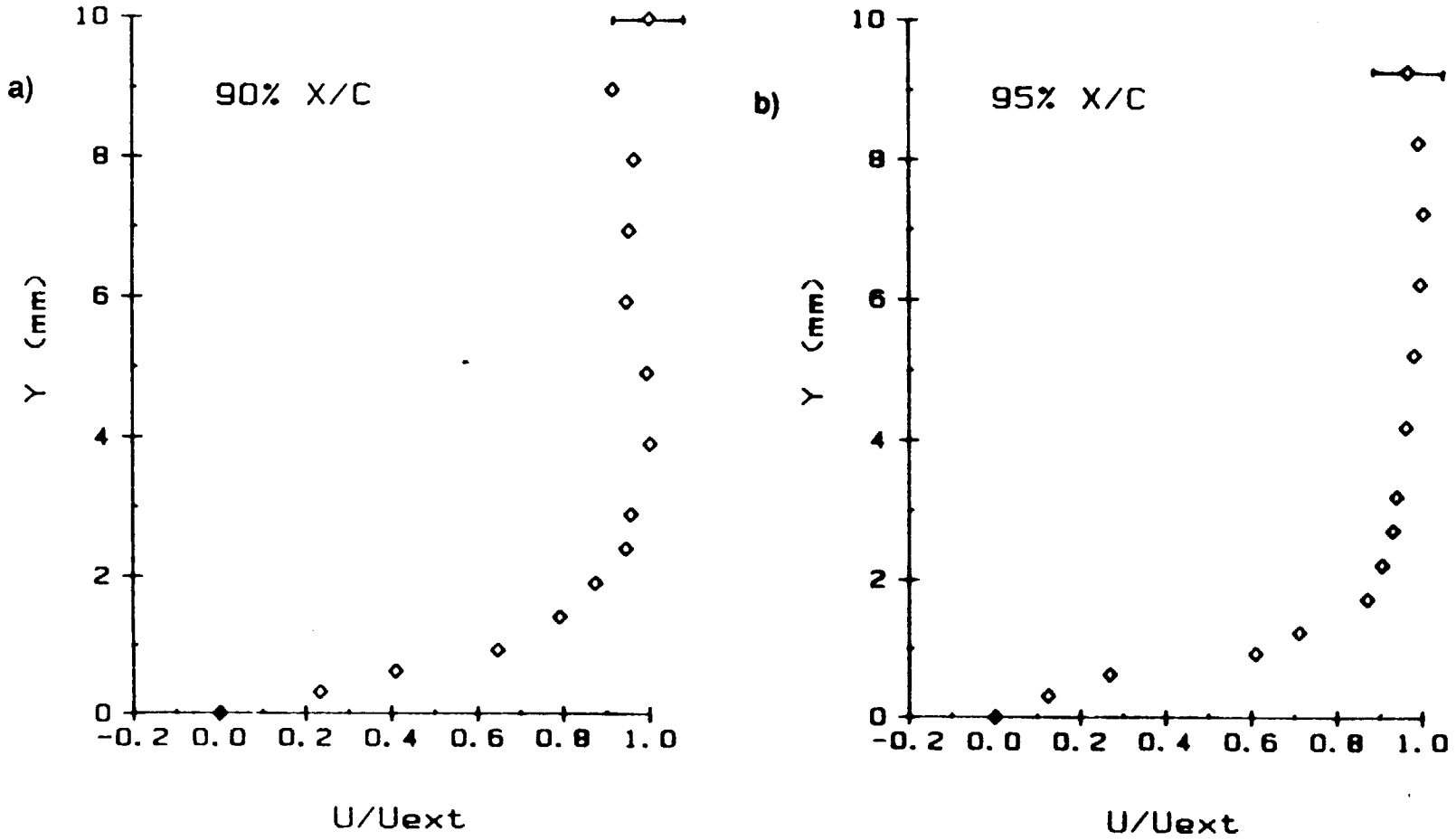

Figure 22 **E387 Airfoil LDV U/U_{ext} Boundary Layer Velocity Profiles, 90% x/c and 95% x/c Chord Positions, R_c = 100,000 , α = 2.0°**

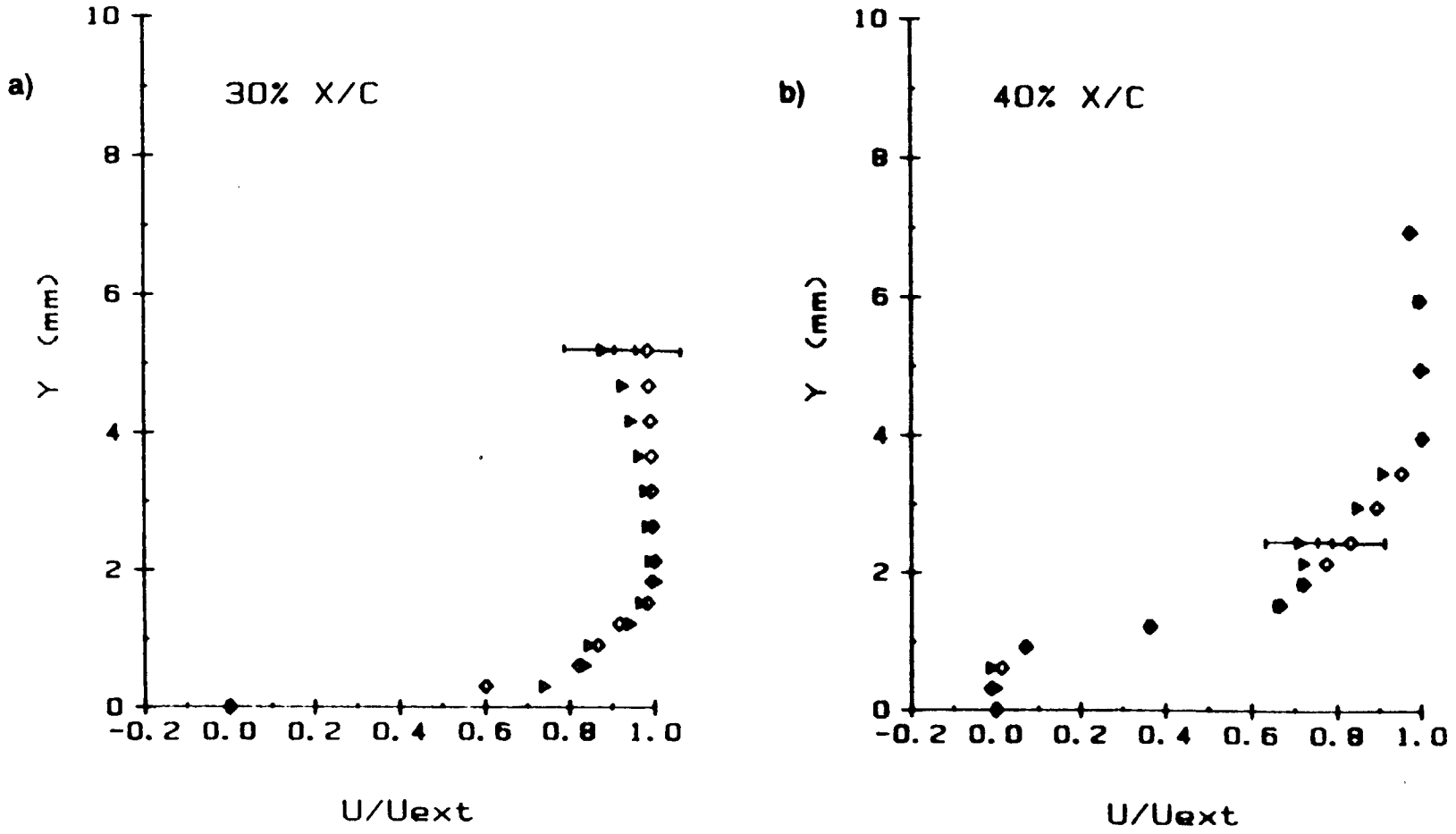

Figure 23 **Repeatability comparison for LDV U/U_{ext} Boundary Layer Velocity Profiles, R_c = 100,000 , α = 2.0°**